

Spheromak Equilibrium Studies on SSX

Cameron Geddes
Swarthmore College Department of Physics

10 June 1997

Arrays of magnetic probes in conjunction with numerical and analytical modeling have been used to study the equilibrium states of magnetized toroidal plasma configurations called spheromaks. A time resolved fit of data to models shows the effects of pressure and current forces in determining the equilibrium, and shows evolution of the state over time. Results indicate a reliable equilibration to a minimum energy state across a range of plasma parameters. Other states are also observed under certain conditions.

1 Introduction to Spheromak Plasmas

A spheromak is a toroid of plasma with toroidal and poloidal magnetic fields of comparable strength generated by currents flowing in the plasma, and with no material linking the center of the torus. The plasma is confined by its magnetic fields, which in turn are held in place by a copper flux conserver. This configuration is illustrated in figure 1. The present experiment, conducted on the Swarthmore Spheromak Experiment (SSX) at Swarthmore College, is a study of the formation and relaxation of such plasmas into a steady state, or equilibrium.

The unique properties of spheromaks have fueled interest in their use for studies of magnetic reconnection and magnetic confinement fusion [Jarboe 1994; Yamada 1990; Ono 1992]. In tokamaks and other conventional plasma confinement schemes, the vacuum vessel is toroidal and field coils thread through the center topologically forbidding extraction of the intact plasma. In contrast, lack of structure linking the center of the torus means spheromaks may be moved after formation, which is useful for these experiments. Magnetic reconnection is a turbulent process involving merging of adjacent parcels of magnetic field. Mobility allows two spheromaks to be formed then (partially or completely) merged to observe this process. Reconnection processes are a candidate to explain the high temperature of the solar corona, and are an important cause of disruptions to plasma confinement in fusion energy reactors. The mechanism behind magnetic reconnection is currently very poorly understood, and there is great interest in exploring it. Low structural requirements and mobility also indicate the potential use of spheromaks as fusion reactors which would have less radioactive structure than tokamak counterparts, and which would take advantage of confinement benefits obtained at low aspect ratio (that is, little or no central structure).

The study of spheromak equilibrium is an interesting problem in basic plasma physics, and is relevant directly to the use of spheromaks as fusion sources since confinement and plasma shape are the primary issue there. These studies are also necessary to lay the ground for reconnection experiments, since in order to study reconnection it is necessary to understand the reservoir of magnetic field available to feed the reconnection region.

The equilibrium project on SSX is a program involving experimental measurements, theory and simulation on spheromak equilibrium, and a set of data processing and fitting tools to allow the theoretical/simulated equilibria to be compared with the experimental results. Various models, which make different assumptions about the spheromak (ie zero pressure for the force free model), also make different predictions about the shape the spheromak's fields should assume in equilibrium. By comparing the predictions of various models

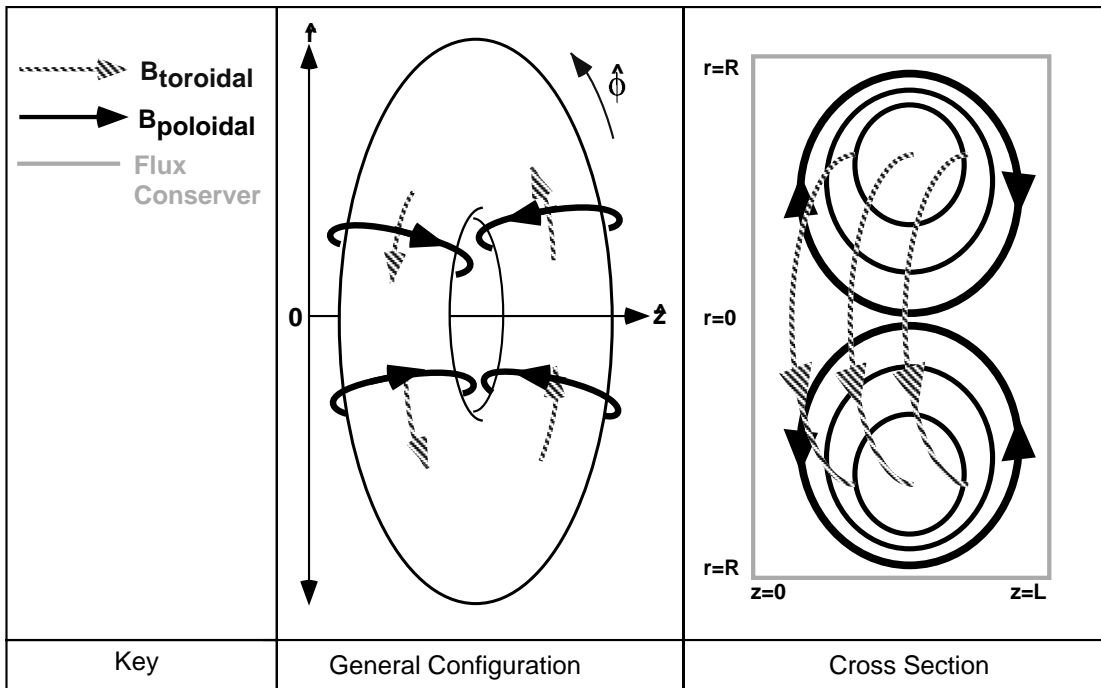


Figure 1: Two views of a spheromak, with the magnetic fields and coordinate axes indicated. Spheromaks usually have azimuthal symmetry, so cylindrical coordinates are used as drawn with z the symmetry axis and with the ϕ axis pointing toroidally around the ring. The cross section at right is taken in the poloidal (r - z) plane. The flux conserver is shown in cross section view only.

with experimental results, we can therefore gain a good idea of the spheromak's characteristics, and of what factors are important in shaping it at various points in its lifetime. By comparing simulations in different flux conserver geometries, we can also determine what effects the flux conserver shape may have on the equilibrium. Such spheromak equilibrium studies have been performed previously [Jarboe 1980; Hart 1983; Knox 1986; Kitson & Browning 1990]. The present experiment uses very high resolution probes and consideration of a wider variety of equilibria. Novel data fitting tools are also used. These methods allow significantly improved precision in identifying and understanding spheromak equilibria. In brief, we find reliable equilibration to a minimum energy state, regardless of changes in start up parameters, and also observe the evolution of the spheromak into other states late in its lifetime. The reasons for this behavior are discussed, and parameters which influence equilibrium are explored.

The remainder of this introduction will give an overview of the interactions of plasmas with magnetic fields, and of the spheromak's formation and characteristics in order to develop background and a qualitative understanding of the important processes. The main body of the paper is then organized into 5 sections. Section 2 describes in detail the theory of plasma equilibrium. In section 3, the computational tools used to simulate equilibrium are described and the results of the simulation program are presented. In section 4, the experimental program is discussed, and section 5 gives an overview of the experimental results and fits to theory. Section 6 is a conclusion and overview.

1.1 Plasma and Magnetic Fields

The interaction between plasma and a magnetic field is the basis of much of plasma physics, including spheromak equilibrium. A plasma is composed of charged particles resulting from the ionization of gas (hydrogen in our case). It is therefore conductive, and may carry an electric current, so its movement will be influenced by a magnetic field, whether externally imposed or generated by internal currents in the plasma.

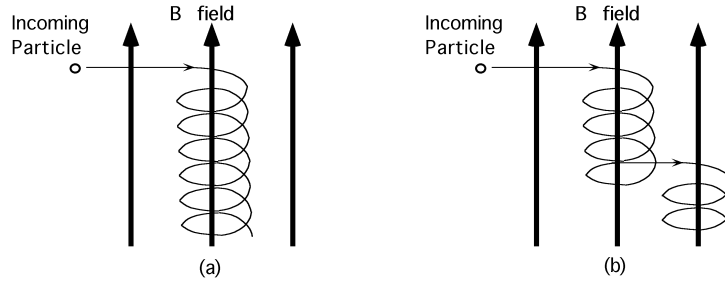


Figure 2: Particle confinement. (a) A particle spirals about a magnetic field line, and will be confined as long as the field lines close on one another. (b) A collision with another particle (not shown) can allow the particle to hop by a distance of one orbital radius from one field line to the next.

There are two primary ways of thinking about plasma-field interactions, the single particle approach and magnetohydrodynamics.

Consideration of a single charged particle in a magnetic field gives a first order idea of the interactions of the plasma with the field. In a magnetic field, a charged particle experiences a force:

$$\vec{F} = q\vec{v} \times \vec{B}$$

This force is perpendicular to velocity, and of constant magnitude, which causes a spiralling of the particle along the magnetic field lines, as illustrated in figure 2. As a result, the particle cannot pass through the magnetic field, but only along it. If a toroidal magnetic field is created with field lines which close upon themselves, the particle will then be forever confined. If the plasma is perfectly collisionless (no resistivity) this will hold for multiparticle plasmas as well.

In real multiparticle plasmas, resistivity is finite and collisions do occur between particles. These collisions can allow the particles to 'hop' outward by one orbital radius, called the 'cyclotron radius'. This radius is simply given by the balance of centripetal acceleration and magnetic force, and is:

$$r_{cyclotron} = \frac{mv_{\perp}}{qB}$$

where v_{\perp} is the velocity component perpendicular to the magnetic field. This process is illustrated in figure 2. Eventually, a random walk calculation indicates that this will allow the particles to escape the field with a characteristic time:

$$t_{diff} = \frac{3\tau R_{field}^2}{r_{cyclotron}^2}$$

where τ is the characteristic time between collisions and R_{field} is the size of the field region (ie the machine radius). This is known as the diffusion time, or confinement time. It is about the maximum amount of time the plasma can be expected to last before escaping confinement.

An alternate view of plasma-field interactions is to think of the plasma as a conductive fluid. This is called the magnetohydrodynamic approach, whether ideal (for infinitely conductive plasmas) or resistive (for resistive (real) plasmas). Consider a conductive fluid with magnetic field embedded in it, called a magnetofluid. If a field line should move with respect to the conductor, this could create a change in flux through that bit of fluid and hence an electric field in the conductor, according to:

$$E = -\frac{d\Psi}{dt}$$

where $\Psi = \int \vec{B} \cdot d\vec{A}$ is the magnetic flux. In a perfect conductor, charges rearrange themselves instantly to prevent any such electric field, and hence any change in Ψ is prohibited. A perfectly conductive plasma is

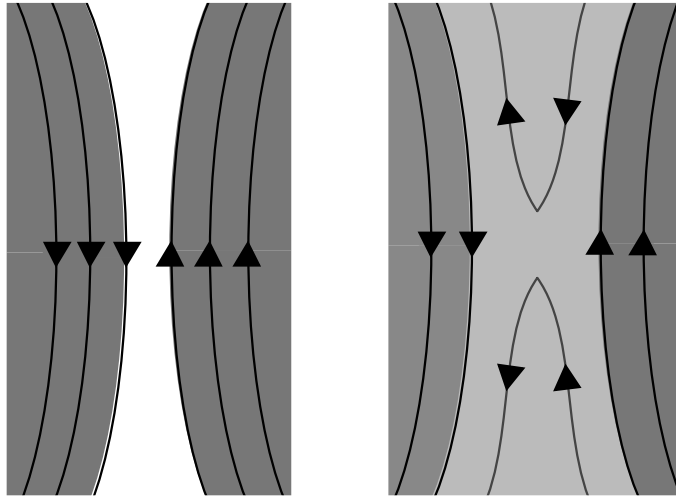


Figure 3: A simple picture of magnetic reconnection. Left: Two parcels of magnetofluid with opposing fields are next to one another. Right: Reconnection between field lines allows dissipation of this unstable state. Reconnected field lines quickly relax away from their highly kinked state, dissipating energy by heating the plasma.

then free to move only along contours of constant flux. Any other movement is prohibited. In this case, no change of the field profiles relative to the plasma can take place, and the initial arrangement of magnetic fields is ‘frozen in’. Since it is a fluid, the plasma can flow and rearrange, but only subject to the condition that each field line remains anchored to the bit of plasma it started with. This imposes severe restrictions on the ability of the plasma to change. It means that the field profiles will remain fixed with respect to the plasma even if they are not close to the minimum energy state. Field lines may also become twisted across one another by movements of the plasma, but still cannot relax.

Resistivity provides two mechanisms for the plasma and magnetic fields to re-arrange and relax to a lower energy state. The first is resistive diffusion. The presence of finite resistivity allows the field lines to move slowly through the plasma on a timescale called the resistive diffusion time or soak time, which just the L/R time of the plasma. In our case this time is tens of microseconds. Since this is shorter than the particle diffusion time, it is the practical limit on the lifetime of plasmas in SSX. Both this process and the particle diffusion process described above are slow and continuous changes in the plasma. Turbulent processes are also possible however, which allow the plasma and magnetic field to re-arrange themselves on a very fast timescale relative to the resistive diffusion time.

Reconnection is the primary turbulent process operative in spheromaks [Barnes 1986]. It is, essentially, the merging of adjacent parcels of magnetic field. This process allows rapid relaxation of the plasma to a minimum energy state. Imagine initially that the plasma moves, carrying magnetic field lines with it (as in the ideal picture). At some point, this movement causes adjacent parcels of magnetic field to be nonparallel, directed across one another. A two dimensional slice of two such parcels is illustrated in figure 3, where for simplicity the fields are shown oppositely directed. When this happens, $\nabla \times \vec{B}$ is very large in the region between the parcels. This is an unstable, high energy condition. The presence of resistivity allows the dissipation of magnetic energy, and therefore permits relaxation of the fields through ‘reconnection’ between adjacent field lines. This process is shown in figure 3. Reconnection allows the field lines to relax, eliminating the region of contrary fields, and therefore rapidly dissipates unstable regions. Energy is dissipated resistively by heating the plasma, and the plasma relaxes to a minimum energy stable state

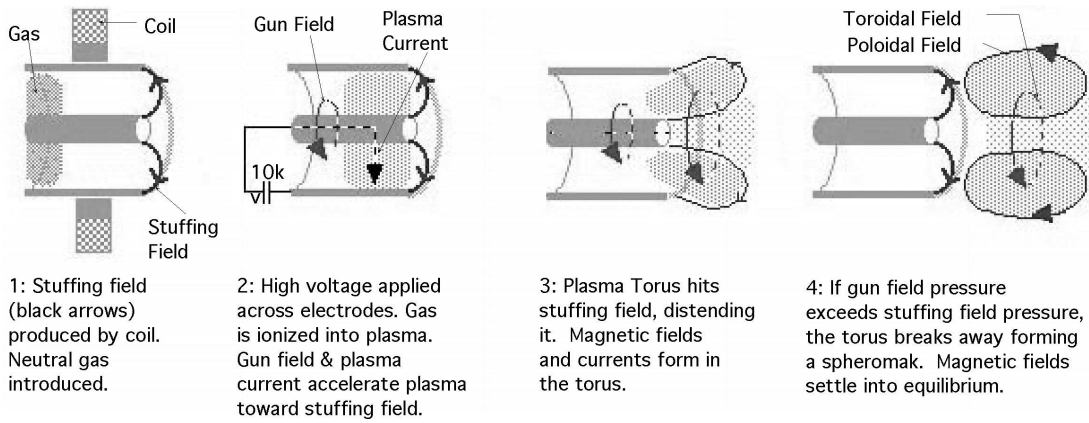


Figure 4: Spheromak formation process. The chamber is shown in a cutaway view, and is physically cylindrical in cross section.

on a timescale short compared with the resistive diffusion time [Taylor 1986]. Some magnetic field is lost by this process, but enough remains to contain the plasma. This is the primary process of equilibration in spheromak plasmas. As mentioned above, the specific mechanism of magnetic reconnection is not well understood.

A small amount of resistivity, characteristic of a plasma, is sufficient to allow reconnective relaxation processes, while preserving the general characteristics of confinement described above. Further, once the plasma has reached the minimum energy state of magnetic field and pressure, reconnection will largely cease, since there is no more energy to dissipate. In that case, the plasma will again be confined by the surfaces of constant flux. Since $\Psi = \int \vec{B} \cdot d\vec{A}$, surfaces of constant flux (flux surfaces for short) also indicate the magnetic field lines. For these reasons, the flux function is the primary indicator of the shape of the plasma, and I'll often refer to it.

If magnetic fields confine the plasma, the next question is what confines the magnetic fields. In a soap bubble, the surface tension of the soap film contains the air with no additional structure. Magnetic fields, for better or worse, do not work this way: since they cannot exert force parallel to themselves, there is no analogue of the surface tension of the soap film. Hence, if nothing holds the fields in place, they will expand under the plasma's pressure without restriction, and the plasma will dissipate. Something must hold the field in place. In a spheromak, this function is typically served by the 'flux conserver,' a closed shell of highly conductive copper into which the spheromak is formed. Just as with the plasma, the highly conductive copper does not allow flux to pass through it quickly, and since it is a solid, turbulent reconnective processes are not possible so that there is no quick way for flux to penetrate. For the SSX flux conservers, the flux soak through time is far longer than the diffusion time of the plasma, and hence longer than the lifetime of the spheromak. On the time scale of the spheromak, the flux conserver then imposes the boundary condition: $\Psi = 0$, or equivalently, $\vec{B} \cdot \hat{n} = 0$ at its walls. Hence, the magnetic field lines cannot pass through the conserver walls, and the plasma's size is limited to the flux conserver volume. Within this volume and boundary condition, magnetic and pressure forces equilibrate.

1.2 Spheromak Formation and Equilibrium

Spheromaks are toroidal plasma rings governed by the plasma - field interactions outlined above. Using these interactions, we can now explore the processes of spheromak formation and equilibrium. Spheromaks are formed in SSX by a magnetized coaxial plasma 'gun,' as illustrated in figure 4. Current flowing in the plasma interacts with the magnetic field produced by the current flowing in the center electrode to produce a $\vec{J} \times \vec{B}$ force which accelerates the plasma towards the opening of the gun. Meanwhile, a coil is turned on which creates a roughly radial field (called the 'stuffing flux') across the gun opening. The plasma,

being highly conductive, resists any change in flux through its surface (as described above). Rather than passing easily through the field, it will therefore distend the field when it hits. If the magnetic pressure of the accelerating field is greater than the magnetic tension of the stuffing flux, the plasma will force its way through the stuffing flux and detach from the gun to form a spheromak. The stuffing flux then ‘reconnects’ behind the spheromak in the manner described above. Some of the stuffing flux remains wrapped around the spheromak, and provides it with poloidal field, while the gun current sets up the toroidal field. In this way, a free floating magnetized ‘bubble’ of plasma is formed. The process is analogous to the blowing of a soap bubble. The soap film tension is analogous to the stuffing flux tension, while the pressure of one’s breath in forming the soap bubble is akin to the magnetic pressure of the gun current.

Equilibrium studies explore what shape the spheromak settles into after formation. Immediately following formation, the field and pressure profiles imposed by the gun are unstable - which is to say they are very far from the minimum energy arrangement. The resistive magnetic reconnection processes outlined above then allow relaxation to a minimum energy state [Taylor 1986]. Resistivity of the plasma ensures that oscillations will be damped. The relaxation will then tend towards a steady state, or equilibrium between magnetic field and pressure forces in which kinks and variations in the field and plasma density are smoothed out. The specific form of this state depends on the relative magnitude of pressure forces and magnetic field forces, and also on the distribution of current in the plasma. The goal of equilibrium studies such as this one is to understand what shape the field and pressure profiles assume in equilibrium, and what factors are important in determining that equilibrium.

Like formation, the relaxation of the spheromak may be usefully understood in analogy to the familiar soap bubble. When a soap bubble is formed, a fixed amount of air is injected into a soap film. The film then soon relaxes into its minimum energy spherical shape subject to the constraint that the amount of air inside stays constant. Similarly, when a spheromak is ‘blown’ into a chamber, a fixed amount of helicity $\vec{K} = \int \vec{A} \cdot \vec{B} dV$ is injected into the magnetized plasma by the gun. The spheromak then relaxes into a (toroidal) minimum energy state subject in this case to constant helicity. Helicity is a measure of the ‘twistedness’ of the magnetic field lines, or in other words the degree to which flux tubes are intertwined with one another. Remarkably, it is conserved even in turbulent conditions [Taylor 1974]. Reconnection in this analogy can be visualized as similar to the merging of two small bubbles (corresponding to parcels of plasma and field) into a larger, lower energy one.

In typical spheromak plasmas, pressure forces are small in relation to magnetic ($\vec{J} \times \vec{B}$) forces. To first order the spheromak can then be considered a minimum energy state of the magnetic fields, subject to the conservation of total helicity and to the boundary conditions of the flux conserver [Taylor 1986]. The minimum energy state can then shown to satisfy the condition:

$$\nabla \times \vec{B} = \lambda \vec{B} \tag{1}$$

λ being a constant eigenvalue dependent on the size of the flux conserver. Equation 1 then determines the form of the magnetic fields and current profiles (see equilibrium theory section, below). The value of λ indicates several characteristics of the equilibrium, including the ratios $\frac{J}{B}$ and $\frac{I}{\Psi}$. The minimum magnetic energy state is found to be a good description of many spheromak plasmas. Because it refers to a state in which pressure forces are insignificant, it is also called a ‘force free’ state. Though it is often observed, variations from this state have been observed in spheromaks due to current distribution and pressure effects.

A few characteristics of the expected solution can be understood qualitatively from what we know so far, and this will serve to develop an intuition for what follows. First, we expect that any flux surfaces that do not close on themselves will not confine any plasma, since the plasma can simply slide along until it escapes. Secondly, since the flux conserver imposes $\Psi = 0$ at its edge, we expect that the field lines should be parallel to it at the edge. A minimum energy state, which avoids large kinks in the field, can then be expected to consist of nested surfaces of flux as illustrated in figure 1. This means we expect $B_{poloidal}$ to reverse sign as we move out from the center to the edge of the toroid, but we expect $B_{toroidal}$ to keep the same sign, again as shown in the figure.

Basic physical principles also allow us to understand the qualitative effect of pressure and current distributions on the shape of the flux surfaces. Adding pressure forces (for instance, $P \propto \Psi$) should cause the flux

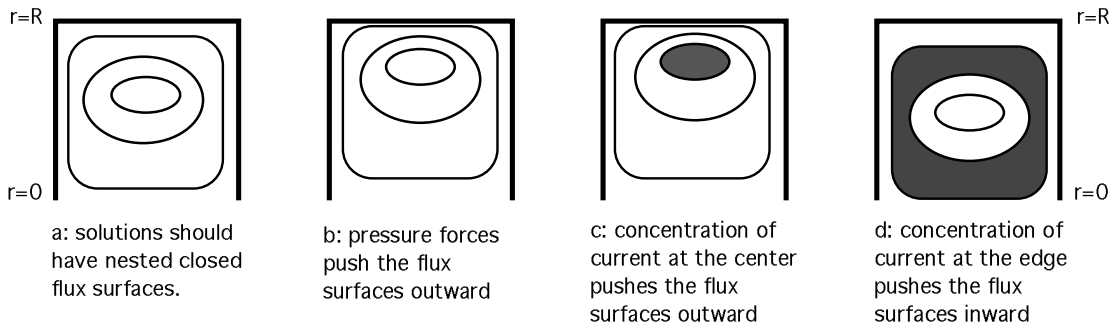


Figure 5: Qualitative ideas about equilibria. Shown is a cut-away view of the flux conserver from $r = 0$ to $r_{max} = R$ in the same poloidal plane shown in figure 1.

surfaces to move outward, in much the same way inflating an inner tube causes it to grow in radius. The reason is that the outside of the flux surface (or inner tube) has more area than the inside, and therefore experiences a larger force due to pressure. What about current distributions? First, think about a circular loop of wire carrying current. Each piece of the wire experiences forces from the magnetic fields of the rest of the wire, and these forces can be shown by $\vec{F} \propto \vec{I} \times \vec{B}$ to stretch the wire out in radius (to convince yourself, think about 2 straight wires carrying opposite currents; these are analogous the two sides of the loop). Going back to the plasma then, current flowing in the plasma should also cause it to try to expand. However, since the flux conserver won't let magnetic field through, the expansion will continue only until the interaction with the flux conserver balances the ring current forces. Let's consider the extreme cases where almost all the current flows on the outside or on the center flux surface. If most of the current flows along the outer flux surface, then that surface would interact strongly with the flux conserver, and would be pushed inward, causing the others to move inward as well. This is called a 'hollow' current distribution. On the other hand, if most current flows on the center flux surface, this surface will drift outward until it interacts with the wall: the flux center should thus move outward in this case. This is called a 'filled' current distribution. Intermediate cases would of course fall in between. These ideas are illustrated in cutaway view in figure 5. It will be important to keep this intuition about the equilibrium in mind to physically interpret the results we see both from simulation and experiment. With this understanding, we are ready to go on to a detailed and quantitative description of spheromak equilibrium.

2 Equilibrium Theory

The equilibrium shape of the spheromak is governed at root by force balance between plasma pressure and magnetic field, which are the two principal important forces in the plasma [Bellan]:

$$F = ma$$

$$\frac{ma}{Vol.} = \frac{F}{Vol.}$$

$$\rho\left(\frac{dv}{dt} + v \cdot \nabla v\right) = -\nabla P + \vec{J} \times \vec{B}$$

and at equilibrium, $a = \text{acceleration} = 0$, so that:

$$\nabla P = \vec{J} \times \vec{B} \quad (2)$$

This is the basic equation used to evaluate plasma equilibrium. The left hand side is simply the force created by pressure gradients in the hot plasma. This force tends to spread the plasma out. The right side is the force of the magnetic fields on the current carried by the plasma. This force resists movement of the plasma across the field, resulting in confinement as long as the \vec{B} fields remain fixed (ie. by the flux conserver). Changing either pressure or current distributions affects the shape of the resulting equilibrium.

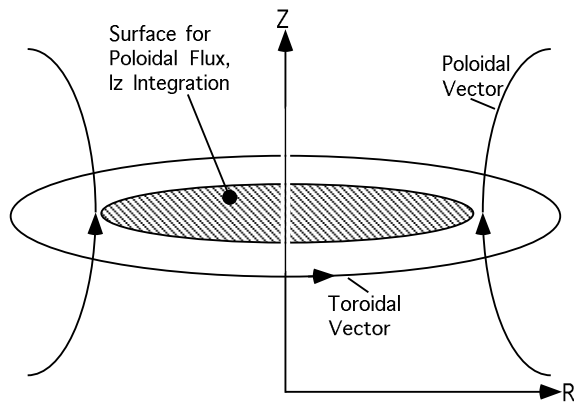


Figure 6: Cylindrical coordinates. The orientation of the coordinates to the spheromak geometry may be seen by comparison with figure 1.

In the form (2), the plasma equilibrium equation is a three dimensional, generally nonlinear and nonseparable partial differential equation without tractable solutions. For this reason, a variety of restrictions are imposed to generate reasonable solutions, which are then compared to experimental results to infer the form of the equilibrium. Force free and Grad Shafranov solutions are the two principle categories of solution relevant to the experiment, and are presented in detail below.

For calculations modeling a spheromak, it is convenient to use cylindrical polar coordinates, and to use the terms ‘toroidal’ to denote vectors in the ϕ direction and ‘poloidal’ to denote those in the $r - z$ plane, as shown in figure 6. The toroidal direction is taken to point around the plasma ring, and the z axis is the symmetry axis as illustrated in figure 1. I will also refer to the poloidal flux, $\Psi(r, z)$ or simply Ψ , which is the integral of poloidal magnetic field over a circle centered at axial location z and with radius r :

$$\int_0^r B_p \cdot dA = \Psi(r, z)$$

which reduces to:

$$\int_0^r B_p \cdot \hat{z} 2\pi r dr = \Psi(r, z)$$

in the axisymmetric case where no variation of the solution in ϕ is allowed. The quantity $I_z(r, z)$, which is the integral of the current $\vec{J} \cdot dA$ over the same circle is also useful. As mentioned above, because magnetic forces act perpendicular to \vec{B} , they also act perpendicular to contours in $\Psi(r, z)$, so that the shape of the poloidal flux function indicates the shape of the equilibrium balance. Also keep in mind that the flux conserver boundary condition is $\Psi = 0$ at the conserver wall.

Because the theory and simulation to follow are motivated by experiments on SSX, it is necessary to have a clear idea of the SSX geometry as well at this point. This is the geometry on which we will need to find equilibrium solutions. Spheromaks at SSX are contained by one of the two flux conservers illustrated in figure 7. Each flux conserver is made of copper and contains the plasma by the processes described above. Both are also axisymmetric, so that equilibrium spheromaks do not usually deviate from axisymmetry. For this reason, solutions will typically be illustrated by a cutaway view of the poloidal flux in the r - z plane.

Though the static equilibrium description applies strictly to a completely unchanging state, in real cases equilibrium will be ‘quasi-static,’ which is to say that there will be slow evolution of the state (generally decay as the plasma escapes and the spheromak dies). If such change is slow enough compared to relaxation times, however, the plasma will be able to remain in equilibrium throughout the change. Hence the equilibrium description will remain valid when changes in the state are slow and continuous.

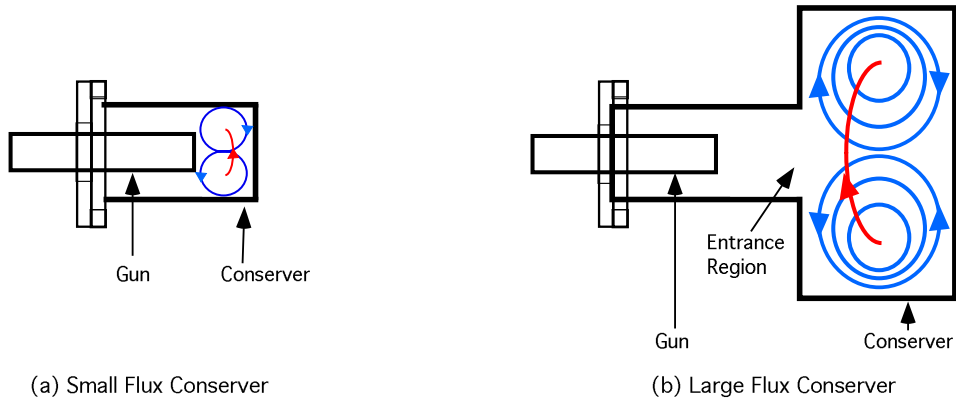


Figure 7: SSX geometry, showing gun and conserver regions in an $r - z$ plane cutaway view. Spheromak flux surfaces are shown schematically in the conserver regions. The flux conservers are cylindrical.

2.1 Force Free Theory

Spheromaks are characterized by low β , or ratio of plasma pressure to magnetic field pressure, because of the requirement that the gun field has to be very strong in order to form a spheromak at all. The simplest equilibrium model is then given by letting $\nabla P = 0$ in (2) above. In practice, this simply means that ∇P forces are so much smaller than $\vec{J} \times \vec{B}$ forces that they do not significantly affect the shape of the equilibrium. In this case, the equilibrium equation reduces to a simple form as follows:

$$\nabla P = 0 = \vec{J} \times \vec{B}$$

and since $\vec{J} \propto \nabla \times \vec{B}$, we have:

$$0 = \nabla \times \vec{B} \times \vec{B}$$

so that $\nabla \times \vec{B} \parallel \vec{B}$ and thus:

$$\nabla \times \vec{B} = \lambda \vec{B} \quad (3)$$

where λ is in general a function of Ψ , possibly but not necessarily constant. Equilibrium is completely determined by the magnetic forces and the relaxation of the magnetic field subject to the boundary conditions of the can at the plasma edge. These solutions are axisymmetric if the flux conserver is.

Constant λ corresponds to the minimum possible energy for the spheromak fields, and this simple model is often an applicable one [Taylor 1986]. It is the same result obtained by the minimization of magnetic energy subject to constant helicity as described in the introduction. The constant- λ force free equation can be solved directly with the boundary conditions of a closed perfectly conductive right cylinder, giving an analytical solution [Schaffer, 1987]:

$$\begin{aligned} B_r &= B_0 \frac{k_z}{k_r} J_1(k_r r) \cos(k_z z) \\ B_t &= B_0 \lambda J_1(k_r r) \sin(k_z z) \\ B_z &= B_0 J_0(k_r r) \sin(k_z z) \\ \Psi &= B_0 \frac{r}{k_r} J_1(k_r r) \sin(k_z z) \end{aligned}$$

where B_0 is an arbitrary constant, and with:

$$k_z = \frac{\pi}{L}, \quad k_r = \frac{3.8317}{R}, \quad \lambda = \sqrt{\frac{k_z^2}{k_r^2} + 1}$$

where R is the radius and L the length of the conserver . Since $\vec{J} = \frac{1}{\mu_0} \nabla \times \vec{B}$, then by (3):

$$\vec{J} = \frac{\lambda}{\mu_0} \vec{B} \quad (4)$$

so that \vec{J} is proportional and parallel to \vec{B} . Constant λ indicates what is called flat current profile, since $\frac{J}{B}$ is constant, and hence $I_z = \int \vec{J} \cdot dA$ is proportional to $\Psi = \int \vec{B} \cdot dA$. Also characteristic of this solution is that the peak flux, which is the point at which B_p reverses sign, is located at $r=0.63R$, where R is the radius of the flux conserver. Complex geometries like that of SSX do not permit analytical solutions and require the numerical methods described below.

Non-constant λ solutions correspond to non - flat current profiles, since variation of λ changes the ratio of \vec{J} to \vec{B} . If λ rises with Ψ , there is extra current density at the flux center, and if it falls with rising Ψ there is extra current at the edge. These states have been used to explain spheromaks in decay or formation/sustainment, not in their lowest energy states [Knox 1986; Kitson & Browning 1990; Browning 1993]. Because the solutions depend on the poloidal flux, they are solved numerically as $P = 0$ cases of Grad Shafranov equilibrium, as described below. They do not have closed form analytical expressions. These solutions show significant deviation from the constant λ force free state, and are also distinguishable from solutions with finite pressure. The flux peak moves outward if λ increases with Ψ (filled current profile; most current flowing at the center), and inward if it decreases with increasing Ψ (hollow profile). The flux surfaces also change shape.

Together, these force free solutions have usually been thought adequate to describe spheromak equilibrium. There are, however, other possibilities if pressure forces become significant.

2.2 Grad-Shafranov Theory

The Grad Shafranov equation is a simplification of the general equilibrium which results from assuming only that the solution is axisymmetric. It allows consideration of arbitrary P and \vec{J} profiles, but assumes that the solution does not vary with toroidal angle. This model describes all stable spheromaks in axisymmetric flux conservers such as ours, and many unstable ones, since the instability is often just movement of the (symmetric) spheromak about the chamber.

A full derivation of the Grad Shafranov equilibrium is presented in Appendix A. In brief, one considers the general form of the axisymmetric magnetic field:

$$\vec{B} = B_p + B_t$$

which can be written:

$$B_p + B_t = \frac{1}{2\pi} [\nabla \Psi \times \nabla \phi + \mu_0 I_z \nabla \phi] \quad (5)$$

as demonstrated in the appendix, where $\nabla \phi = \frac{\hat{\phi}}{r}$. Since $\vec{J} = \nabla \times \vec{B}$, we can also write:

$$\vec{J} = J_p + J_t = \frac{1}{2\pi} [\nabla I_z \times \nabla \phi - \frac{r^2}{\mu_0} \nabla \cdot (\frac{1}{r^2} \nabla \Psi) \nabla \phi] \quad (6)$$

Inserting this into the equation (2) for the equilibrium, we obtain:

$$\nabla P = (J_p \times B_t) + (J_t \times B_p) + (J_p \times B_p)$$

where the last term points in the toroidal direction and is therefore 0 by axisymmetry, since no change in P is allowed in the toroidal direction. Since J_t and B_t are parallel there is no $(J_t \times B_t)$ component. Inserting the expressions for \vec{B} and \vec{J} into this equation shows that ∇P and ∇I_z are both parallel to $\nabla \Psi$ so that P and I_z are functions of Ψ . The equation can then be reduced to:

$$\nabla \cdot (\frac{1}{r^2} \nabla \Psi) + 4\pi^2 \mu_0 P' + \frac{\mu_0^2}{r^2} I_z I_z' = 0 \quad (7)$$

where 's indicate derivatives with respect to Ψ . This is the Grad Shafranov equilibrium equation. Note that the equation is now in terms of Ψ and functions of Ψ , confirming that the poloidal flux is the significant parameter.

Though simpler than the full equilibrium equation, the Grad Shafranov equation is a nonlinear equation in Ψ which has no general analytic solutions. Because it involves three independent quantities, Ψ , $P(\Psi)$, and $I_z(\Psi)$, it also does not uniquely determine the equilibrium. In order to use the equation, two of functions (usually $P(\Psi)$ and $I_z(\Psi)$) are specified and the remaining one can be solved for. This means that in order to fit experimental data from magnetic probes (which measure Ψ), one must guess at reasonable pressure and current profiles. A set of solutions is created and fitted to the data, and the best fit is picked. An iterative computer program can do this by taking an initial guess at equilibrium and adjusting parameters until it finds a best fit. Solutions to the Grad Shafranov equation are, with few exceptions (such as the force free solution shown above), impossible to compute analytically, so numerical simulation is used to generate solutions. The simulation and fitting programs are described in a separate section below.

The force free solution is simply a special case of Grad Shafranov equilibrium with $P = 0$. The current distribution is determined by equation 4:

$$\vec{J} = \frac{\lambda}{\mu_0} \vec{B}$$

Then we have:

$$I_z = \int \vec{J} \cdot dA = \int \frac{\lambda}{\mu_0} \vec{B} \cdot dA$$

In the constant λ case, this becomes simply:

$$I_z = \frac{\lambda}{\mu_0} \Psi, \quad I'_z = \frac{\lambda}{\mu_0}$$

indicating that the current is proportional to the flux. A similar integration can be performed to find the appropriate current distributions for variable λ states.

When considering variable λ states, it is convenient to express λ as a power series in Ψ , and usually only the first order term is relevant. This yields [Knox 1986]:

$$\lambda = \bar{\lambda} \left(1 + \alpha \left(2 \frac{\Psi}{\Psi_{max}} - 1 \right) \right)$$

where $0 \leq \alpha \leq 1$ governs the dependence on Ψ , and where $\bar{\lambda}$ is the average value of λ over the plasma. It is usually of the same order as the constant λ value calculated in the analytic solution, but is found precisely by trial and error numerically. If α is positive, center current is increased relative to edge, which is typical of spheromaks in decay, since the edges are cooler and more resistive than the core. Negative α corresponds to excess edge current, typical of spheromaks still being driven by the gun, while zero α is the fully relaxed state corresponding to constant λ . Using this form has the advantage that it guarantees that λ does not reverse sign. Sign reversal in λ would correspond to a reversal of current direction, which is unstable and not generally physically observed, so it is desirable to exclude it. A similar convention can be used when second order in Ψ is desired, yielding:

$$\lambda = \bar{\lambda} \left(2 + \alpha \left(2 \frac{\Psi}{\Psi_{max}} - 1 \right) + \gamma \left(2 \left(\frac{\Psi}{\Psi_{max}} \right)^2 - 1 \right) \right)$$

The process can of course proceed to arbitrary order in Ψ as needed. Higher order in Ψ allows description of more sharply peaked current distributions, whether of filled or hollow type.

Integration yields the desired current distributions for variable λ without difficulty. For first order solutions in Ψ , this is:

$$I_z = \int \vec{J} \cdot dA = \int \frac{\lambda}{\mu_0} \vec{B} \cdot dA$$

$$I_z = \frac{\bar{\lambda}}{\mu_0} \left(1 - \alpha + \frac{\alpha \Psi}{\Psi_{max}} \right) \Psi$$

$$I'_z = \frac{\bar{\lambda}}{\mu_0} (1 - \alpha + 2 \frac{\alpha \Psi}{\Psi_{max}}) = \frac{\lambda}{\mu_0}$$

Similarly, for second order in Ψ , we obtain:

$$I_z = \frac{\bar{\lambda}}{\mu_0} (2 - \alpha - \gamma + \frac{\alpha \Psi}{\Psi_{max}} + \frac{2\gamma \Psi^2}{3\Psi_{max}^2}) \Psi$$

$$I'_z = \frac{\bar{\lambda}}{\mu_0} (2 - \alpha - \gamma + \frac{2\alpha \Psi}{\Psi_{max}} + \frac{2\gamma \Psi^2}{\Psi_{max}^2}) = \frac{\lambda}{\mu_0}$$

Since for force free solutions λ is proportional to the ratio between \vec{J} and \vec{B} (that is, to I'_z), it is a convenient and physically meaningful parameter that can be used to characterize the solution.

For finite pressure solutions, pressure profiles are also written as power series. However, since $P = 0$ outside the outermost flux surface (no confinement), there is no constant term, so that:

$$P = P_1 \Psi + P_2 \Psi^2 + \dots$$

Particle transport by the random walk process described above tends to even out sharp kinks in the pressure distribution. In most cases, therefore, each flux surface contains an equal amount of pressure, so that only the linear term is needed. The presence of pressure also complicates the current distribution. By substituting the Grad Shafranov equation (7) back into the expression for toroidal current (6), we obtain a new expression for J_t and hence for total \vec{J} :

$$J_t = (2\pi r^2 P' + \frac{\mu_0}{2\pi} I_z I'_z) \nabla \phi$$

$$\vec{J} = J_p + J_t = \frac{I'_z}{2\pi} \nabla \Psi \times \nabla \phi + (2\pi r^2 P' + \frac{\mu_0}{2\pi} I_z I'_z) \nabla \phi = 2\pi r^2 P' \nabla \phi + I'_z \vec{B}$$

$$\vec{J} = J_p + J_t = 2\pi r^2 P' \nabla \phi + \frac{\lambda}{\mu_0} \vec{B}$$

where the last term is the force free current. In order to facilitate comparison with force free solutions, I will characterize finite P solutions by λ and P profiles, but it is necessary to remember that λ no longer completely determines J_t (though it will be close for small β). J_p remains of the same form as in the force free case. Combinations of linear P and quadratic λ profiles are sufficient to cover equilibria in the present experiment. In general arbitrary order can be used, but higher order corrections are within our experimental error, so they are not considered.

Finding equilibrium solutions through the Grad Shafranov equation is an excellent way of exploring the behavior of the spheromak. By generating solutions with various pressure and current distributions and observing the ways in which the solution changes, we can understand how altering these distributions changes the equilibrium. Because we must guess at solutions to generate fits to data however, it is often a less than efficient method for analyzing experimental results.

2.3 Grad Shafranov Solution Extraction

In the special case where we are able to collect data on vector \vec{B} on a line all the way across the machine from $r = 0$ to $r = R$, there is a more efficient way of fitting theory to experiment than guessing at solutions and searching for a best fit as described above. In this case, one can find Ψ by:

$$\Psi(r) = \int_0^r B_z(r') 2\pi r' dr'$$

and using the above formula for B_t (5):

$$B_t = \frac{\mu_0 I_z}{2\pi r}$$

$$I_z = \frac{2\pi r B_t}{\mu_0}$$

This specifies two of the three quantities required to solve the Grad Shafranov equation, and P can then be obtained by re-arranging the equation to yield:

$$\frac{-1}{4\pi^2\mu_0}[\nabla \cdot (\frac{1}{r^2}\nabla\Psi) + \frac{\mu_0^2}{r^2}I_z I'_z] = P'$$

Numerical integration then yields P from P' , completely specifying the equilibrium. I refer to this method as ‘extraction’ of the solution from experimental data, as distinct from simulation and fitting of a possible solution.

The extraction process requires high radial probe resolution in order to return reliable results. Insufficient resolution or accuracy can cause the integral to yield $\Psi \neq 0$ at $r = R$, a condition forbidden by the flux conserver. The $\frac{1}{r^2}$ term in the derivative of Ψ causes further problems near $r = 0$. Though matters can often be improved by fitting a polynomial to $\vec{B}(r)$ to smooth the data, this is not always sufficient. Because it involves fewer steps, it is almost always possible to extract Ψ and I_z , while a precise P profile is often difficult to obtain. Even if a precise pressure profile cannot be obtained, however, one can usually find a ‘typical’ value of P' which can allow calculation of a rough pressure. Since pressure effects are usually small in spheromaks, the precise form is not very important and this is enough to be quite useful.

When it can be used, extraction yields a simple one step method of obtaining an equilibrium fit. Because it exactly fits to the actual data, extraction also achieves a precision which is practically impossible with guessing methods. It can therefore reveal small deviations from the force free state or from constant λ which would otherwise be missed. Conventional solutions as described above are still quite useful in order to provide a basis of comparison, to allow exploration of various states, and in cases when the extraction method does not work. The two methods may be used in conjunction, with extraction used to obtain P , I profiles which can then be plugged into a conventional method to obtain a solution, which is usually an excellent fit to the data. The two methods also cross-check each other in this way, offering a robust way to connect theory with experimental data.

2.4 Instability

In some cases, the equilibrium as described by the above equations may not be entirely stable. There are a number of so called ‘instability modes’ which describe common behaviors in which the spheromak does not settle into a fixed and stationary state. A few examples include the tilt, in which the spheromak flips on its side in the conserver, rotational modes in which the entire spheromak rotates around the chamber, and modes in which it wobbles up and down or side to side. Most of these modes consist of motion of the spheromak in the chamber, while the shape of the equilibrium is otherwise undisrupted. Some of these modes are illustrated in figure 8. The tilt instability is controlled in SSX by shaping of the flux conserver, and will not appear. Other instabilities are detectable by looking at signals at various azimuthal or radial locations and searching for a signal variation that rotates or oscillates from one probe to the next.

3 Simulation

Very few solutions to the Grad Shafranov equation can be computed analytically, and none are possible with complex geometries like those of the SSX flux conservers. For this reason, equilibrium solutions are found numerically by the use of a finite element method partial differential equation (pde) solver based on MATLAB software running on a PowerPC. The finite element method is a method by which the differential equation is calculated on a discrete grid of points. From an initial guess solution, the solver alters the solution iteratively until it obtains a solution with error less than some preset condition. This allows solution of a wide variety of equations and boundary conditions, including the Grad Shafranov equation. As mentioned

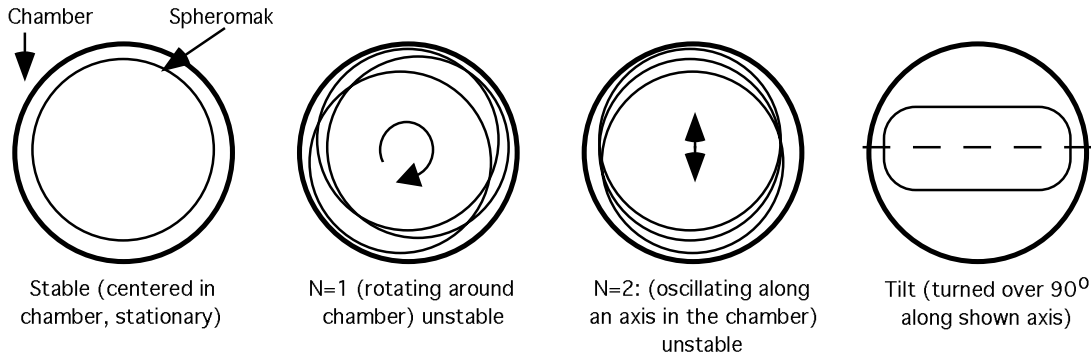


Figure 8: Spheromak instabilities illustrated. The view shown is looking down the z axis.

above, we can generate a series of solutions by this method both to explore possible equilibrium states and to deduce the form of the experimental equilibrium by finding which solution best fits the data.

The MATLAB pde toolbox is capable of solving a variety of equations in 2D cartesian coordinates. The general form of the equation that can be solved is:

$$-\nabla \cdot c \nabla u + au = f$$

where a , c , and f are coefficients and u is the quantity to be solved for. When the coefficients depend upon u , the equation is nonlinear and a nonlinear solver is used. The Grad Shafranov equation is recast into X,Y coordinates from R,Z to accommodate the solver, becoming:

$$\nabla \cdot \frac{1}{y} \nabla \Psi + \frac{\mu_0^2}{y} I_z I'_z = -4\pi^2 \mu_0 P' y \quad (8)$$

where $y = r$ and $x = z$, $u = \Psi$ and $-\frac{1}{y} = c$. ∇ is the cartesian del operator. One can easily see the equivalence between this form and the cylindrical one (7) by writing the operators out in component form. I usually choose $\frac{\mu_0^2}{y} I_z I'_z = au$ and $-4\pi^2 \mu_0 P' y = f$ for the remaining coefficients, since this allows easy modeling of force free and linear pressure states. It also allows modeling of other states while keeping the coefficients to lowest possible order in Ψ , which is desirable from a computational complexity point of view. The solver allows simulation of arbitrary geometries and boundary conditions. This allows us to compare equilibria in a ‘perfect’ closed cylinder with those in the actual SSX geometry. We can then evaluate how the different flux conserver and entrance region shapes and sizes used on SSX (see Figure 7) affect the equilibrium.

3.1 Issues in Numerical Solution

The major problem inherent in numerical techniques such as the Finite Element method is forcing the solver to pick the proper solution when more than one solution is numerically valid. In particular, the equation:

$$\nabla \cdot \frac{1}{y} \nabla \Psi + \lambda^2 \Psi = 0$$

which is the force free equation expressed as a case of the Grad Shafranov equation has as solutions both the (desired) solution displayed below and also the zero solution. Since the zero solution is completely error free, the solver will always converge on it. This problem can also cause distortions of finite pressure solutions, since the solver will ignore any term in the solution that can be set to zero. To solve the problem, a tiny perturbation is applied to the boundary so that $\Psi_{edge} \neq 0$, though Ψ_{edge} will still be much less than Ψ_{max} . This makes the zero solution invalid, and the solver will now pick the proper solution. Solutions with nonzero pressure do not change at all as Ψ_{edge} is varied as long as $\Psi_{edge} < 0.1\% \Psi_{max}$. The perturbation can be very small in these cases, so $\Psi_{edge} < 10^{-90} \Psi_{max}$ is chosen. Solutions with zero pressure (force free cases)

vary only in magnitude as Ψ_{edge} is varied, but since these solutions can be scaled arbitrarily while remaining valid, this is not a problem. The boundary perturbation in these cases is about $10^{-8}\Psi_{max}$. Stability of the solutions when Ψ_{edge} is changed indicates that these perturbations are not affecting the solution and are mathematically valid ways of obtaining convergence.

Another solution convergence problem arises when there are more than one nonzero functions which satisfy the equation, as occurs in some force free solutions with variable lambda. In this case, whichever is favored by the initial guess and the solver's convergence condition will be selected. Then one must find some error condition which is satisfied by one of the solutions and not the other. Fortunately, the 'lower' solution, which converges with the normal error condition, is the physical one in our case so that this is not a difficulty.

A difficulty specific to the Grad Shafranov equation is that since the equation contains a factor of $\frac{1}{r}$, solutions tend to infinity at $r = 0$. Though a human can easily set appropriate conditions for an analytic solution (ie $\Psi = 0 @ r = 0$), the computer is not good at this, especially when the equation is nonlinear. For this reason, r_{min} is set to $0.005r_{max}$ rather than zero. As with the boundary flux perturbation, this does not affect the solution. This is again verified by comparing solutions with various r_{min} values and observing that changing r_{min} does not affect the solution as long as $r_{min} < 0.01r_{max}$.

In addition to the fact that the perturbations are small and varying them does not affect the solutions, there are other reasons to believe that they produce accurate results. The numerical solutions are checked against analytical solutions when available, for instance with the force free solution. These comparisons indicate that the numerical solver is accurate. Further, an independent 'checker' program has been written which can evaluate the Grad Shafranov equation numerically at each grid point in a solution. This checker verifies the simulation results, giving an entirely independent check on the simulation. Lastly, when data are fitted to these solutions, we check the solution parameters which give the best fit against those derived from data by the extraction program, which is a third independent code. Hence we have good confidence that the results of the program are accurate.

The last potential difficulty lies in the guessing nature of the program. For simple solutions where the coefficients do not depend on Ψ , the solver can find the solution from an initial guess of a constant. For nonlinear solutions however, especially force free variable lambda solutions, this is not good enough. In this case, an iterative method is used. A case which is close to the desired one and which can be solved from the ground up is done first. Then this solution is used as an initial guess for the solution desired. In some cases, multiple steps must be made, each one serving as the initial guess for the next, until the desired solution is reached.

3.2 Solutions

A range of solutions have been calculated within the parameter space defined in the equilibrium section, linear pressure profiles and quadratic current profiles in Ψ . These serve to illustrate the behavior of the solution under various conditions of pressure and current distribution. Solutions have also been calculated in various geometries including a perfect cylinder and the two flux conservers used on SSX.

First, let us consider the effects of device geometry, using the force free solution as an illustration. Figure 9 shows three solutions generated in the two SSX flux conservers (illustrated in figure 7) and in a 'perfect' closed cylinder geometry. The closed cylinder and large flux conserver solutions are negligibly close to one another, with very small distortions only at the edge of the entrance region. The flux surfaces do not protrude significantly back into the gun entrance. This is a result of the entrance region being a small aberration in a large conserver. In contrast, the small flux conserver is not a good approximation of a closed cylinder geometrically, and this clearly affects the solution significantly. Most importantly, the spheromak does not center in the conserver. The flux maximum (B_z reversal point) sits at $z = 0.42 L$, rather than at $z = 0.5 L$ as it does in both the perfect and LFC geometries. This means that a probe placed at $z = 0.5 L$ will see a small nonzero B_r in the small flux conserver, but zero B_r in the others. The flux maximum does not move radially in any conserver. This has an important consequence: since simulation in a closed can requires as little as a third of the computer time of true geometry simulations, we can accurately and beneficially use

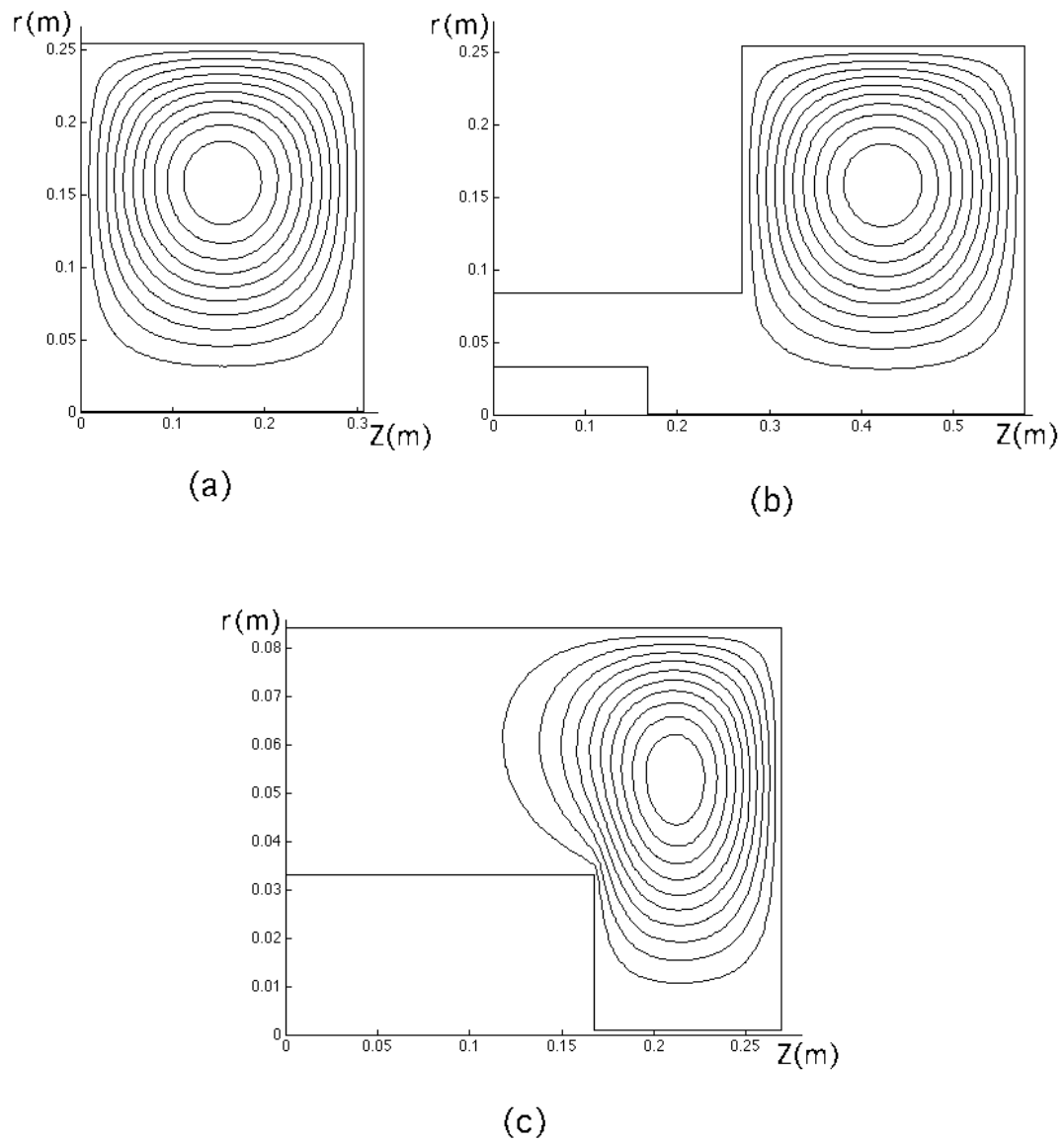


Figure 9: Effects of geometry on the solution. Solutions for the poloidal flux (a) in a perfect can, and (b) in the SSX large converter are similar, while a solution (c) in the small converter is distorted, protruding more into the gun region.

this geometry to do fits in the large conserver. This will not be possible in the small flux conserver.

Physically the above has indications for the behavior of the spheromak in different geometries. In the large conserver, with its small sharp entrance region, the spheromak completely detaches from the gun, while in the small conserver a significant portion of flux remains in the gun. Though more detailed exploration would be required, this implies that conserver/gun interfaces can be tailored effectively to allow the total detachment of the spheromak (ie for reconnection) or to keep it connected to the gun (ie for continued current drive). A transition which does not require large kinks in the field lines for connection (the SFC) will allow this, while a sharp boundary will promote the disconnection from the gun (LFC). This is intuitively reasonable, since kinks in the fields will tend to be unstable and will be ironed out by reconnection. Since the eventual goal of the SSX large flux conservers is to study reconnection with minimum gun interference, this is a favorable result.

Consider next the selection of solutions with various P and I distributions. Since it has been used for most of our experiments, the large flux conserver (approximately closed can) geometry will be assumed for these solutions. Small flux conserver solutions show qualitatively the same results.

Force free states are expected to account for most spheromak behavior, so we focus on them. For the constant λ force free state, agreement with the analytical solution is obtained at the value $\lambda_0 = 18.21$ which results from applying the analytic solution's formula to the SSX conserver dimensions. This confirms that the solver is working properly. Since it is the minimum energy state, we expect this state to appear following the spheromak's initial relaxation. Variable λ force free states with positive α , corresponding to filled current distributions, can account for spheromaks in decay. Some trial and error is needed to determine the resonant value of $\bar{\lambda}$ in these cases, since it is not exactly equal to the constant λ value. When positive α states are computed, one can observe the shifting of the flux center out from 0.63R (the constant λ value) to .67R at $\alpha = 0.98$. Second order solutions push the flux center out yet farther. The flux surfaces re-shape to accommodate this change, with the resulting changes in magnetic fields. Plots of several representative force free solutions are shown in figure 10. We do not sustain the spheromak, so that detachment from the gun occurs early and the plasma settles rapidly into a constant λ state after formation rather than a negative α state which might correspond to current continuing to be driven on the outer flux surfaces.

If the value of λ is varied in the simulation of force free states, a strong resonance in the solution is noted at some value of λ , at which point the maximum flux increases towards infinity. For constant λ , this value is just $\lambda = \lambda_0$, and for variable solutions it changes from this value somewhat. This resonance has been observed before [Browning 1993], and corresponds to the fact that at $\lambda = \lambda_0$ the field is essentially an eigenmode of the cavity. This has several important implications. The solution is scalable arbitrarily at this (and only this) value of λ . The solver picks the largest possible flux in this case since doing so minimizes the error to solution ratio. Scalability of the solution was verified by using the checker program. This characteristic is convenient for fitting, since the solution can be calculated once and merely scaled to match the observed field sizes. It is shared by all force free states, and again agrees with the analytic expression at constant λ . It is interesting to ask what the physical implications of the resonance and scaling behavior are. Scalability indicates that adding or subtracting energy simply causes the state to vary in magnitude, rather than changing its form, so that the spheromak can decay or grow (if driven) while staying in the same state, which is not possible with other solutions. This may account for some of the stability of these states. If there is a physical resonance to correspond to the mathematical one, the resonance in Ψ and therefore in field strength at λ_0 would correspond to an infinite energy barrier since $E \propto B^2$. States of $\lambda > \lambda_0$ would then be energetically forbidden. Such states are not experimentally observed, confirming this prediction, so it is possible that simulation mirrors reality here. The resonance behavior also has implications for the effects of pressure on the state. These will be explored in the analysis of the finite pressure solutions.

The simplest finite- pressure solution is the so called Solov'ev solution. Without boundary conditions, this is one of the few analytic solutions that can be computed to the Grad Shafranov equation. It has the I' , P' profiles:

$$I' = 0, \quad P' = \text{constant}$$

which is to say linear pressure in Ψ (which is fairly realistic) and all the poloidal current flowing along the outermost flux surface (which is very unrealistic except perhaps at startup). Comparison of analytic solution

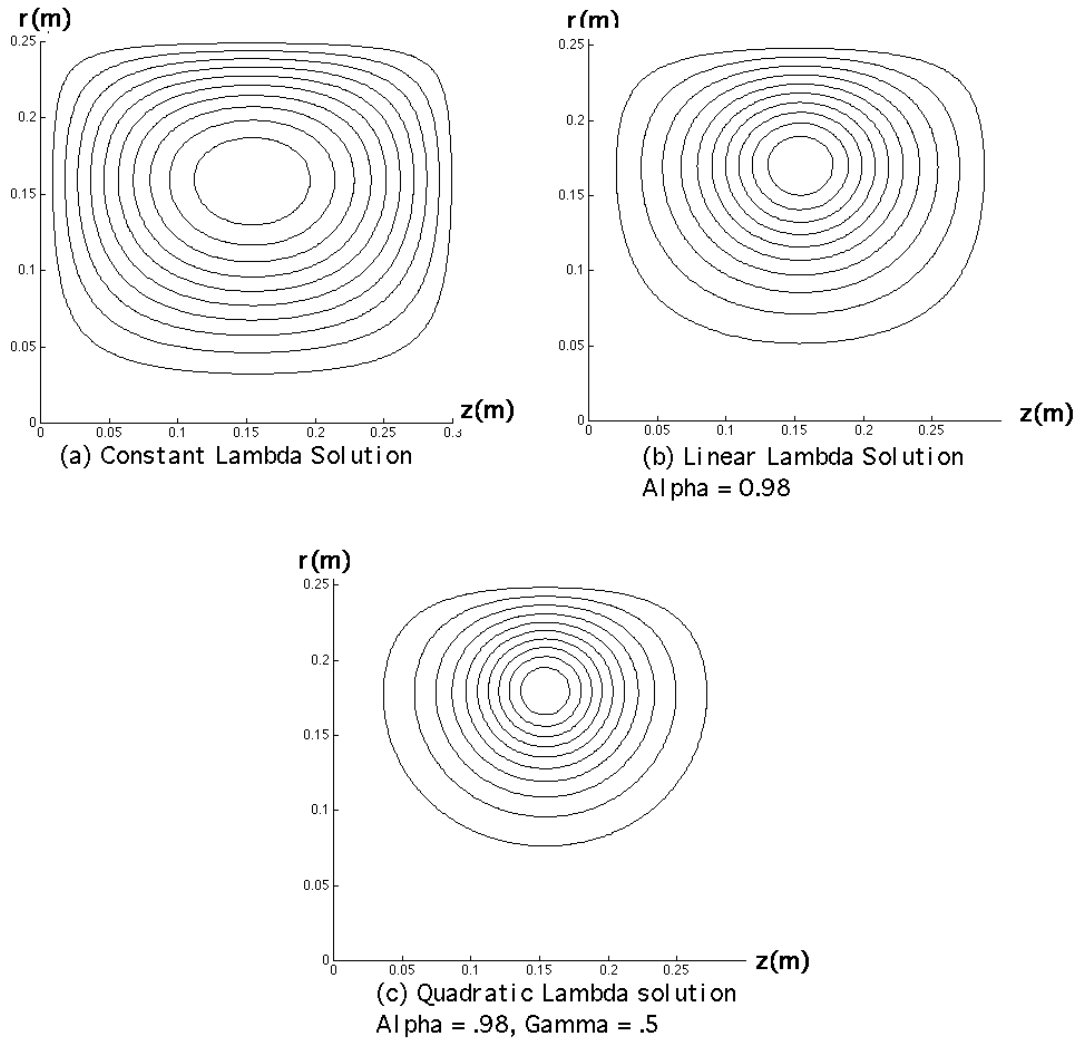


Figure 10: Force Free Solutions for the poloidal flux with various λ profiles.

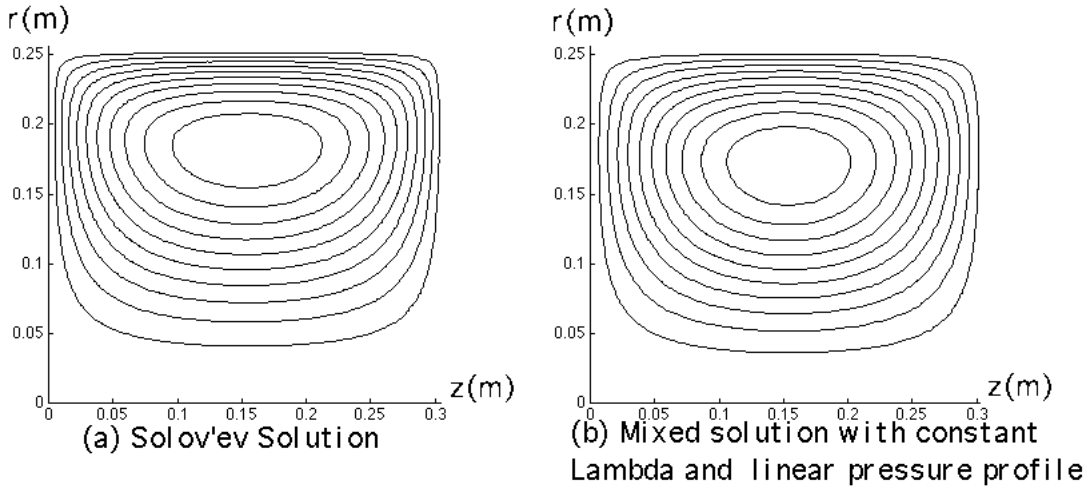


Figure 11: Finite Pressure Solutions for the poloidal flux.

to the numerical solutions with boundary conditions can be made in the $z=L/2$ plane, where the boundary conditions do not change the solution. This again verifies that the solver is accurate. The flux reversal point in either case is always at $r=0.73R$, regardless of P or I magnitudes. A solution of this type is shown in figure 11 along with other finite pressure solutions. Finite pressure solutions are never arbitrarily scalable, and resonance is not observed. This is true both of Solov'ev and other finite pressure solutions.

The above solutions each vary one of the P or I profiles, while restricting the other to 0. It is also possible to solve more physically relevant profiles, with both P and I profiles to first order in Ψ (though higher orders are possible with this method, they are not needed to fit experimental data). Depending on the pressure and current terms, the solutions in general will fall somewhere between the relevant Solov'ev and force free equilibria. One such solution is displayed in figure 11. This solution has a flat current distribution (like the constant lambda force free solution) and a linear pressure profile (like the Solov'ev solution). It shows a flux reversal point between $.73R$ (Solov'ev) and $.63R$ (Force free constant λ). By generating a series of such solutions, a fit to experimental data can be found.

If the current term has λ at a resonant value, the resonance strength will effectively prevent the pressure from having any effect on the equilibrium over reasonable ranges. These solutions are *not* scalable, so this is not a mathematical artifact of the solver. If the simulation accurately reproduces physical reality, this extreme stability to disruption may account for the excellent agreement of many spheromak experimental equilibria with the constant λ state, which is the state with the strongest such resonance. The physical basis of the stability is probably that the constant λ eigenvalue state represents a minimum energy state of the fields, so that moving away from it may be energetically costly. This would be expected to result in the observed stability to disruption. Varying λ by a small amount also does not disrupt the state, indicating that it is stable to current perturbations as well.

A few general features of the solutions are worth summarizing. As expected from the qualitative analysis above, solutions with finite pressure or filled current distributions show outward movement of the flux center compared with force free (zero pressure) constant λ solution. This is in agreement with other simulation codes [Knox 1986; Browning 1993]. Some force free solutions have the same flux reversal point as some combined (finite pressure) solutions, but the shape of the flux surfaces is different due to the forces of pressure distending them in the latter case so that the solutions can in principle be distinguished. However, sometimes the poloidal field solutions may be very close to one another, and may fall within the fit error. Fortunately, the ratio of poloidal to toroidal field also changes with pressure, allowing one to distinguish the states. Since the derivative of flux is determined by both pressure and current, adding pressure increases Ψ_{max} for a given I_z distribution. Since B_t depends only on I_z while B_p depends on Ψ , this means that while

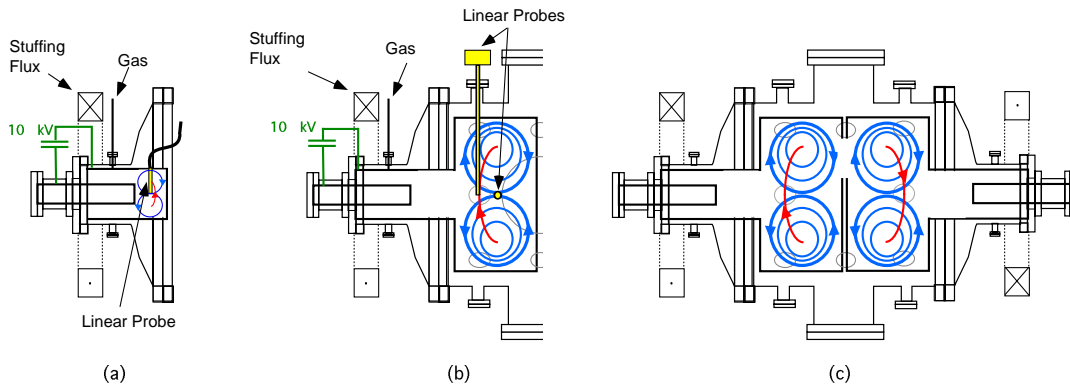


Figure 12: A schematic of the SSX gun showing (a) small and (b) large flux conservers and the magnetic probes for equilibrium work. (c) shows both guns set up with two large flux conservers to allow reconnection studies. The reconnection region is the cutaway in the upper inside walls of the flux conservers.

force free solutions have roughly equal toroidal and poloidal field magnitudes, finite pressure solutions have relatively more poloidal field. This gives a good first-glance way of evaluating the importance of pressure forces in the equilibrium, and of distinguishing solutions. The quantity:

$$\beta = \frac{2\mu_0 P}{B^2}$$

which is the ratio of plasma pressure to magnetic pressure, is a useful measure of whether pressure effects are significant. Pressure effects can be seen when β exceeds about 10%. Below this point, they are not distinguishable.

4 Experimental Setup and Program

Equilibrium measurements have been made on the Swarthmore Spheromak Experiment (SSX) at Swarthmore College. The SSX laboratory consists of a dual magnetized plasma gun system. A schematic of the vacuum vessel and guns is shown in figure 12c. Only one gun is currently operational to create plasmas for equilibrium studies. Either a small flux conserver (12a) with $r_{cons} = r_{gun} = 8.41cm$, and $L_{cons} = 10.2cm$, or a large flux conserver (12b) with $r_{cons} = 25.4cm$ and $L_{cons} = 30.8cm$ can be installed. The gun regions are identical in both conservers to facilitate scaling studies and comparisons between the results. Most operation has been in the large flux conserver, with the small conserver used only for preparatory work. The two guns can be fired simultaneously to create two spheromaks at once so that interactions can be observed (figure 12c).

Four Northstar Research capacitive power supplies are each capable of delivering 25kJ of energy over about $25\mu s$ to the gun, while a separate system provides up to 3.7mWb of stuffing flux through the external coil. Typical plasma parameters are shown in table 1. These parameters give us access to a plasma regime which is highly comparable with solar flare conditions, in line with the eventual goal of the lab to study such phenomena.

Measurements are made by a set of linear magnetic probes along with a digital signal processing package

density	$10^{15} cm^{-3}$
temperature	10 eV
B(characteristic)	0.2 Tesla
Beta	10%

Table 1: SSX Plasma Parameters

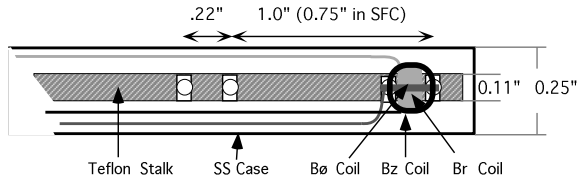


Figure 13: Schematic cutaway of linear probes

designed to optimize their accuracy and precision. Data are interpreted with the aid of a time resolved fit code which fits simulation results to experimental data. These systems are outlined below.

4.1 Magnetic Probes and Data Processing

The probes consist of two linear arrays mounted in the SSX large flux conserver or one in the small conserver as shown in figure 12. Each array in the large conserver consists of 11 sets of three orthogonal coils of #40 magnet wire wound on a custom machined teflon stalk and mounted in a vacuum proof stainless steel housing, as illustrated in figure 13. In the small flux conserver, a smaller probe with 5 coilsets is used. By Faraday's law, the voltage produced by each coil is proportional to $\frac{d\Phi}{dt} = NA \frac{dB_{\perp}}{dt}$, so that the coils measure the time derivative of \vec{B} , which can be integrated to obtain magnetic field. The stainless steel casings are quite thin and not highly conductive, so that the time for flux to soak through them is very short compared to relevant measurements (less than $0.1\mu s$) and does not affect the probes. Each coilset measures three axes simultaneously, so that vector \vec{B} is measured at 11 radial locations and at two locations along the length of the machine and around it toroidally, for a total of 22 simultaneous measurements. Radial sensitivity is emphasized since it is most crucial to determining the shape of the equilibrium, while some z resolution is often helpful in order to allow us to distinguish equilibria which differ from one another mostly away from the symmetry axis. Toroidal offset of the probes allows us to watch for rotational or shaking instability modes more effectively as well.

A significant problem in the construction of accurate magnetic probes is ensuring that the three axes are perpendicular. Irregularities in winding and flexibility of the coil form, especially at the very small coil sizes required to minimize plasma disruption, result in cross-coupling between axes on the order of 10%. Though this may seem like a small issue, in fact it can cause significant problems when the signal on one axis is very much larger than that on another, since the coupled signal from the stronger axis will completely overwhelm the desired signal on the weaker one. This is a problem for instance at the edge of the flux conserver or at $z=L/2$, where $B_r \approx 0$, but B_z and B_t are large. In the present experiment, a simple technique has been devised which eliminates this problem, allowing recovery of signal without cross coupling to within $< 1\%$. After assembly but before insertion, a Helmholtz coil is used to apply a known field along each axis to the probe, and the response of each sensor coil in signal per unit \dot{B} on each axis is determined, giving for each coilset a matrix such that:

$$KB = S$$

where B is the time derivative of the magnetic field vector, S is the signal vector, and K is a matrix such that K_{ij} equals signal on the i axis due to unit \dot{B} on the j axis. Then by inversion:

$$B = K^{-1}S$$

where K^{-1} is the inverse of the $\frac{\text{signal}}{\dot{B}}$ matrix obtained above. These matrices have been calculated for all coilsets, and are automatically applied to correct the signal by the processing software. This method completely compensates for coil misalignment, twisting of the form, and so on. The mountings of the top (foreplane) probe are very rigid and allow little twisting of the probe, so mounting alignment is not an issue. The midplane probe must on the other hand be flexible in order to reach the proper z location, though it can be rigidly fixed once installed. The alignment is therefore re-verified after insertion by inserting a Helmholtz coil through the gun opening. The accuracy of the signal is then only limited by the accuracy with which

we can acquire signals which is better than .1%, or the accuracy of alignment of the calibration field which is about $\theta \approx 0.5^\circ$, corresponding to a cross talk error of:

$$\frac{B_{\perp} \cdot dA}{B_{\parallel} \cdot dA} = \frac{B \sin(\theta)}{B \cos(\theta)} = .008$$

resulting in a total cross talk error of about 1%, which should not interfere with measurements except at the wall or precisely at $z=L/2$ where Br should be exactly zero. In those places, small deviations from zero are likely to be cross talk error.

Due to the short ($100\mu s$) lifetime of the spheromak, integration of the \dot{B} signals to recover magnetic field is a significant problem. Signals can be integrated either with the use of analog RC integrators, or by sampling \dot{B} at a high rate (with an RC filter to remove the highest frequency noise) and digitally integrating the signal in post processing. Each technique has its difficulties. Since noise is eliminated and the integrated signal changes more slowly, analog integrators allow use of slower digitizers. However, they cause loss of signal intensity and can ‘droop,’ causing signal distortion due to the discharge of the capacitor. On the other hand, digital integrators offer great precision, but since errors in the sum will propagate they require high sampling rates. SSX has 32 channels of 10MHz digitizers, and four at 50MHz. The 50MHz digitizers are easily fast enough to digitally integrate, and the 10MHz units can do so with some signal processing, so this method is chosen. The 10MHz digitizers are ‘corrected’ by forcing the integral (ie B) to zero at the beginning and at end of the run after the \dot{B} signal returns to zero. This must be true physically since there is no field before or after the experiment, and it is verified by the faster digitizers. A correction is then applied to the rest of the signal to make it fit these conditions. This process produces good agreement with the faster digitizers. It is incorporated into the same automatic signal processing code which applies the cross-calibration matrix corrections. Despite these steps, however, integration is the least accurate step in our data acquisition, with possible errors as high as 10%. In order to detect ground loops and possible HV shorts of the probes to the casing, the processing code also looks to make sure all the probes zero out at about the same time. A suspicious probe is flagged allowing the experimenter to evaluate it.

There is always concern, when inserting probes into the plasma, that they will disrupt it so much as to invalidate measurements. Tests in the small flux conserver seem to indicate that this is not a significant problem however. Tests were first run with a small ‘nub’ probe which extended only 1/4” into the conserver, which should have very little effect. The same type of runs were repeated with the long linear array. No shortening of lifetime was observed, and signals were similar to within shot variability limits, indicating that there was not significant disruption. Since the probes are smaller in relation to plasma size and energy in the large than in the small flux conserver, we expect that disruption should not be an issue there either.

4.2 Fitting the Data

As outlined in the simulation section, we have two ways of connecting experimental data with theory. One is the use of a fit code which compares simulated solutions with experimental data. A time resolved fit code is used which finds a rough fit to the data of a few basic models (force free constant λ and Solov’ev) at about 100 time points, giving as output a QuickTime movie of the experimental fields and fits. This allows us to identify the times at which the spheromak is stable for more detailed analysis. Then, a specific fit can be done to data at a certain time to show detailed information about the equilibrium. This fit is adaptive and seeks the best fit to the data by continuously adjusting I and P distributions until a best fit is obtained. It is more precise but also much more computationally intensive, so that it can only be done at selected times. We also use the extraction method outlined above to derive Ψ and I_z profiles directly from data and to infer P profiles. These profiles are compared to the results of the other fit methods to provide a cross checking of the fit. This dual method yields high confidence in the identification of the equilibrium states and forces.

5 Experimental Results

Equilibria have been measured in SSX over a range of experimental parameters. Gun voltage and stuffing flux are the two significant variables governing the formation of the spheromak and its characteristics. This experiment has characterized spheromaks with gun voltages from 3kV to 5kV (energies of 4 to 10 kJ) and stuffing fluxes between 1 and 2.5 mW in both flux conservers. Lower energies are not found to form spheromaks with stable equilibrium phases. These measurements have been fitted to the simulation results as described above so that we can see how the spheromak evolves over time for various start up parameters.

5.1 Large Flux Conserver Results

Most data have been collected in the large flux conserver, and this is where the most interesting and relevant equilibria are observed. This conserver is also identical to that which will be used for reconnection experiments, so the results apply directly to characterizing the reconnection flux reservoir. A typical run, which displays the main characteristics observed, is described in detail, followed by a discussion of trends in the data.

A representative run is shown in figure 14. This spheromak was fired in the large flux conserver with 5kV of gun voltage and 1.5mW of stuffing flux, a setting which was observed to produce long lasting, high field plasmas. It displays three characteristic phases which are typical of many runs; formation, constant λ force free state, and a decay state.

Immediately after formation until about $45\mu\text{s}$, the field profiles are chaotic, and change rapidly (figure 14a). The midplane probe measures $B_r \approx B_z$, indicating that the spheromak is not yet equilibrated in the center of the FC. The poloidal field changes rapidly as the two sets of plots show, and the change is often sudden rather than continuous. In this phase, the poloidal field does not integrate to zero, indicating that there are open flux lines which do not wrap all the way around the spheromak. The toroidal field at first appears to approximate a center wire current, as a result of the fact that it is indeed set up by the gun current which is in effect a center wire. The toroidal field is also stronger than the poloidal at this time. As time passes, the toroidal field evolves away from the center wire distribution and the poloidal field becomes more settled. Both evolve towards the force free minimum energy state. This is the manifestation of the relaxation process described in the introduction.

After the chaotic relaxation phase, the spheromak settles into a state which is a very good fit to the force free constant λ state calculated above. The extract program also verifies that $\lambda \approx 18m^{-1}$, which is the expected value, and λ varies only by about 10% across the machine. Pressure is also small relative to magnetic field ($\beta \leq 10\%$). This phase lasts from approximately 52 to $67\mu\text{s}$ and is shown in figure 14b. It occurs significantly after the peak fields, which is to be expected since the chaotic reconnective phase should dissipate some of the magnetic energy. In this phase, poloidal field integrates out very close to zero, indicating that flux contours are closed and the spheromak is fully formed and detached from the gun. Toroidal and poloidal field are very close in magnitude, indicating that the relaxation of toroidal into poloidal flux has occurred and that the state is very close to force free. Further, as time passes, the field profiles change only slowly and continuously, indicating that quasi-static equilibrium is established. Also in this phase, radial field decreases to about 10% of B_z with the occasional exception of the $r = 0$ reading. This indicates that the spheromak is approximately centered in the conserver. Small deviations from zero radial field are likely due to integration errors. There are no high frequency oscillations in the magnetic fields, indicating that the spheromak is stable. The spheromak now begins slow decay.

As time progresses, the poloidal field reversal point, where B_z is zero, moves outward in radius from $0.63R$ to $0.71R$, as illustrated in figure 14c. The peak in toroidal field also moves outward. Two factors may contribute to this effect. If pressure effects are becoming significant, this may move the flux center outward and produce the observed effect. This may be reasonable since the plasma is being resistively heated through its lifetime, potentially increasing pressure effects at the same time magnetic fields are becoming weaker. Alternatively, we may be observing a force free state with nonconstant λ . If increased resistance in the cool

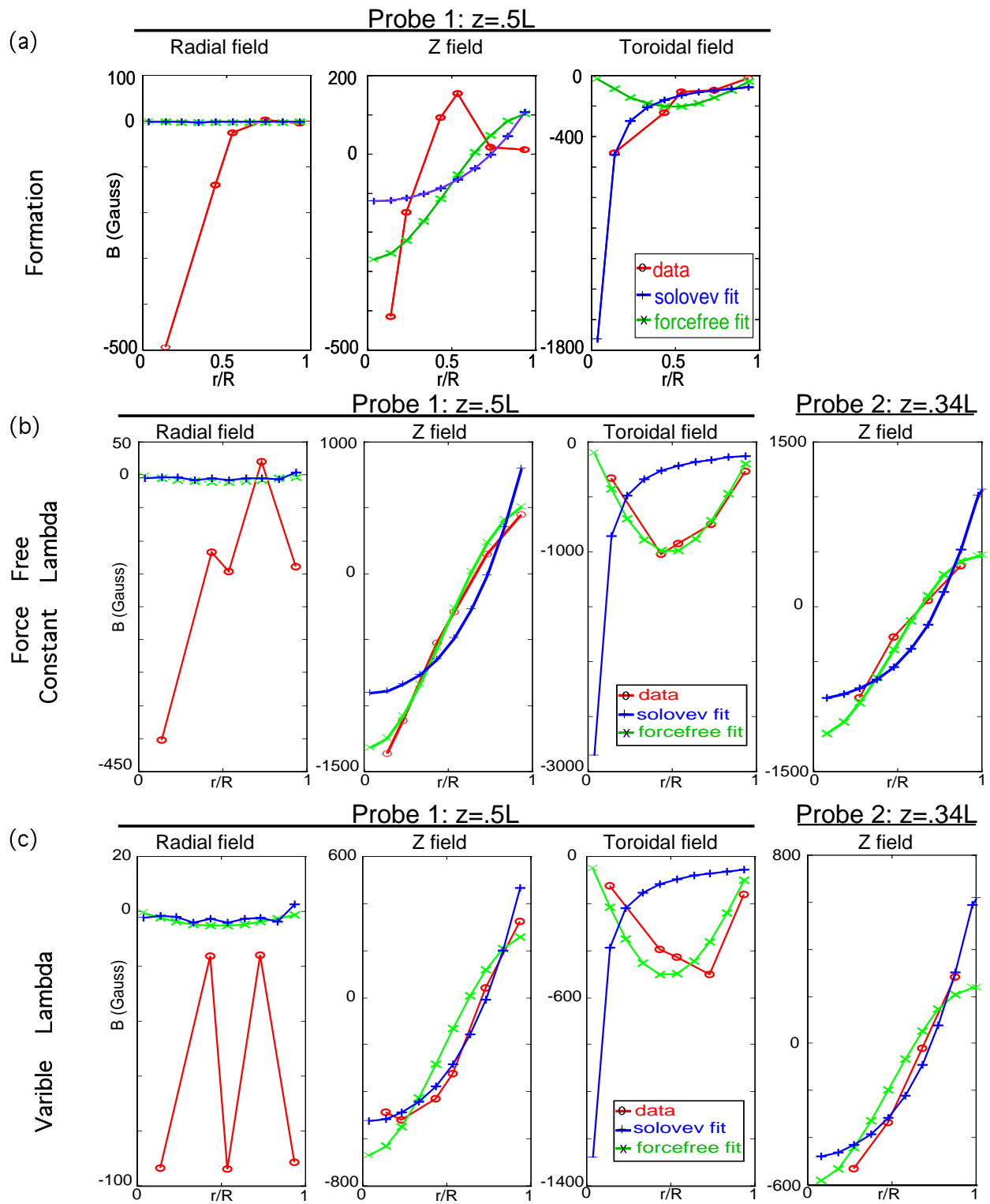


Figure 14: Representative Run: Large Flux Conserver. Magnetic field profiles and fits to simple models are shown at the three major phases of development: (a) formation, (b) force free equilibrium, and (c) variable λ equilibrium. The force free fit is to the constant λ state in all fits shown.

edges of the plasma causes current to fall off faster there, which is likely, then we will end up with a filled current profile state as described above. If so, it must be a second order state, since no first order force free solution has a flux reversal point at such large r . Of course, the observed profile may also be a combination of these effects. Since the toroidal and poloidal field magnitudes remain comparable, however, it is likely that this is an approximately force free state with little pressure effect. A full fit to models verifies that it is not possible that pressure effects can cause the flux center movement. The extraction program also yields $P' \approx 5 \times 10^5 \text{Pa/Weber}$, corresponding to a β of about 10%. This is likely to be too weak to have a significant effect on the equilibrium. A quadratic lambda profile (peaked current distribution) model is then likely appropriate, with perhaps a small contribution from plasma pressure. The extract program yields a fit for $\lambda(\Psi)$, which gives $\bar{\lambda} = 9.6m^{-1}$, $\alpha \approx 0.0$, and $\gamma \approx 0.97$, confirming the expectation of quadratic λ and low pressure.

Though we find that pressure effects are not likely to be prominent in any of the states, it is emphasized that this result is not conclusive. We have no direct pressure diagnostics, only what we infer from magnetic data. The problems noted above with the extraction program are prominent here, and the value of P' is not precise. However, the simulation program confirms that it should not be possible to have ratios of poloidal:toroidal field as close as we observe with much higher β , so there is also good reason to believe our result is accurate.

As gun voltage and stuffing flux are varied, many characteristics of the spheromak remain constant, but there are also interesting differences. The turbulent phase is always observed, as is equilibration into an initially constant λ force free state. This consistency confirms that spheromaks are in fact roughly force free minimum energy states of the magnetofluid following formation. It is also important since it establishes the stability of the force free state, which will be used as the reconnection flux reservoir. Reliable settling into this predictable, stable state will be a great asset in these experiments. As one would expect, higher settings of gun voltage produce higher field spheromaks which last longer due to higher temperature and therefore lower resistivity. At any given gun voltage, there is an optimal setting of stuffing flux to produce the biggest, longest lived spheromak. At higher fluxes, the spheromak barely detaches and is weak. At lower fluxes, the decreased flux level leads to lower poloidal field and weaker confinement. The differences in behavior are principally associated with the decay modes. At high energies, filled current distribution states are observed, as described above. The extent to which the current distribution peaks in this state increases with energy, and to some extent varies from run to run (probably due to wall conditioning). At low energies, below 4kV, the second equilibrium phase is not observed, and only the constant lambda force free state is present. This may be because at lower energies the magnetic field dissipates completely before resistive effects have a chance to change current distributions.

These results can be compared to those of other researchers who have studied spheromak equilibrium. Kitson & Browning [1990] and Knox [1986] have both seen evidence of variable λ states in decaying spheromaks, but found that only first order variable λ forcefree states were distinguishable. In contrast, we find strong evidence for quadratic profiles in some cases. Wysocki [1988] and Hart [1983] have seen evidence for significant pressure effects, which we do not observe. Also in contrast to other researchers [ie Knox 1986], we do not see instability modes even in the decay phase, though this may in part be because of lower plasma energy density as compared to other machines.

5.2 Small Flux Conserver Data

A preliminary data set was collected in the small flux conserver with the goal of exploring scaling and flux conserver shape effects. The data show very different trends from those observed in the large flux conserver however. No long term stable equilibrium phase is observed at all in the small flux conserver. The spheromak lives only about 20-40 μ s, and never settles into a state which can be matched by a reasonable pressure or current distribution. The flux maximum point is at approximately $r=0.5R$, but never stabilizes, and flux surfaces do not close (figure 15). Radial field is much larger than expected, even including expected distortion due to the (relatively) larger opening into the gun. A look at the equilibrium solution in figure 9 suggests that since the equilibrium protrudes into the gun, perhaps current is still being driven.

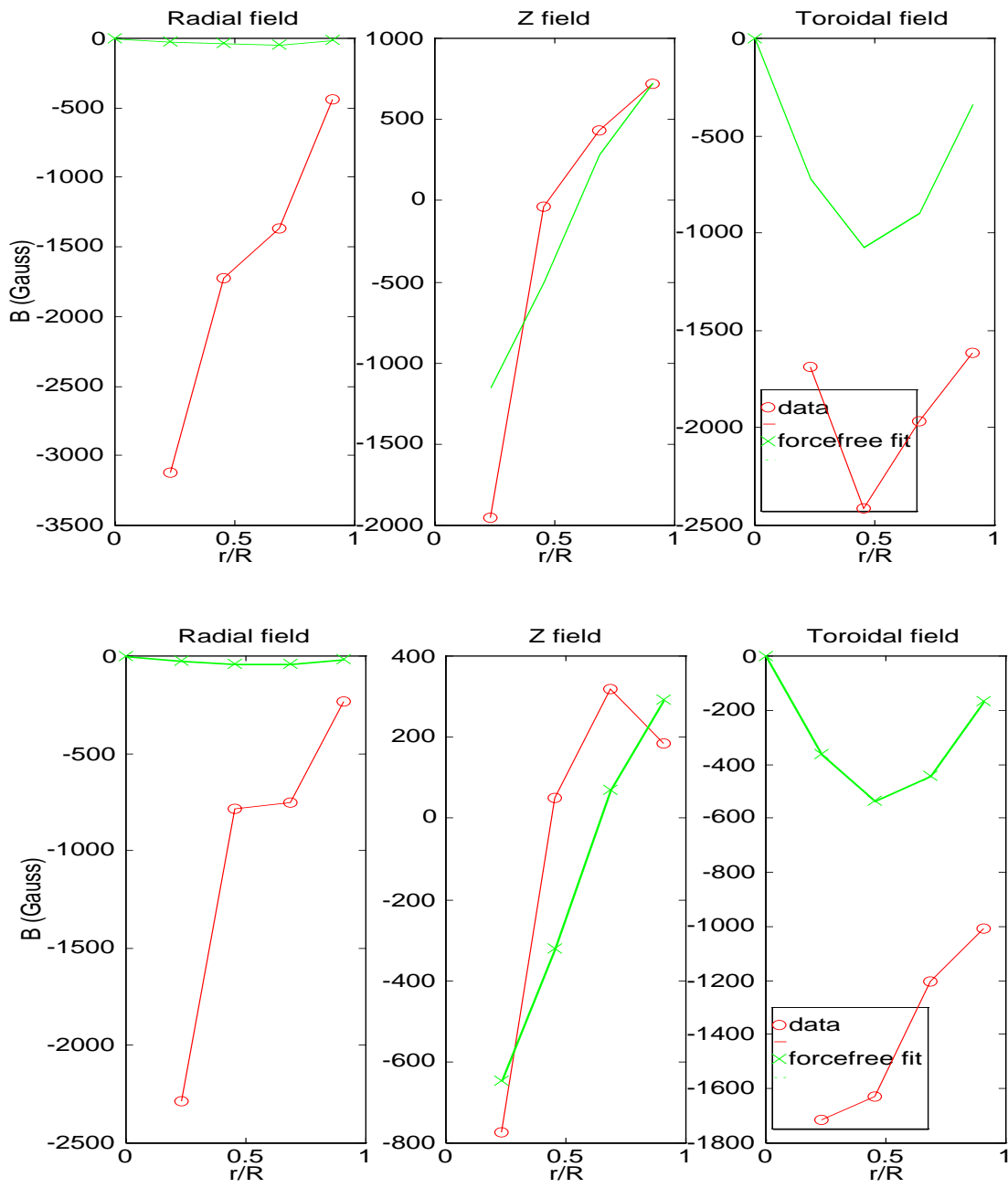


Figure 15: Representative Run: Small Flux Conserver. Fits at $31 \mu s$ (above) and $38 \mu s$ (below) show large radial field and rapid change, not equilibration.

Indeed, looking at the power supply current waveform shows that current is large and changing rapidly throughout the lifetime of the small conserver spheromak. The fact that toroidal field retains a center - wire like distribution also implies continued gun current. Though equilibrium is possible with current drive (spheromaks have indeed been sustained this way), the fast changing current and short lifetime in this case do not seem to allow enough time for this to take place. The manner in which fields change does become more continuous later in the life of the spheromak, but never fully settles down. A short lifetime is expected, since the smaller radius leads to a smaller inductance and a shorter L/R time. However, power supply current reversal due to inductive ringing may further cut this short, since it would cancel out currents in the plasma rather than reinforcing them. Indeed, we see that the spheromak reliably dies at about the time that this occurs. It seems that this and the rapidly changing current drive are enough to prevent stable equilibrium from developing. It was speculated that the stuffing flux field might be distorting our measurements, but including this field did not remedy the problem. Preliminary data thus indicate that the small flux conserver is not a suitable equilibrium spheromak system. This seems to illustrate the importance of the significant gun-to-conserver break present in the large flux conserver, as well as large enough size (and therefore inductance) to allow equilibration. A more complete study would be necessary before drawing conclusions however.

6 Concluding Remarks

In this project I have used both numerical modeling and experimental measurement to understand the equilibrium states and evolution of spheromak plasmas. The results show a turbulent phase immediately following startup, which corresponds to a reconnective relaxation process. This is followed by reliable equilibration to a force free minimum energy state. This state is observed regardless of startup parameters, offering strong confirmation of the idea that spheromaks are minimum energy plasma configurations at least initially. After this phase, slow quasi-static evolution to a second equilibrium phase sometimes showing highly peaked current distributions is observed. In contrast to others' results, we do find that second order current distributions are sometimes significant, especially late in the lifetime of the spheromak. We do not believe that we observe significant effects of plasma pressure on the equilibrium.

A flexible simulation program has been developed which allows modeling of spheromaks with various pressure and current distributions, and with axisymmetric flux conservers of arbitrary shape. This program has been used to generate solutions which illustrate the behavior of spheromaks with various current and pressure distributions. One notable result has been to show the extreme stability of the force free constant λ state to disruptions by pressure or current distribution changes. This stability is likely a reflection of the fact that the state is a minimum energy state, and it also explains why this state describes spheromaks so well. It is also of note however that this stability makes it difficult to identify whether plasma pressure or slightly nonconstant λ distributions are present at all, since their effects are small. Fits to various models might not distinguish these effects, even though they may be present. Hence one must be cautious in identifying states on this basis. Simulation has further aided in a tentative explanation for the strange small flux conserver data in terms of gun-spheromak coupling. This code can easily be used to project the behavior of spheromaks in new geometries, or under current drive or other conditions. This makes it useful for future design efforts. Basing the code on MATLAB technology able to run on most computers makes the code widely accessible. Restricted computer power and some idiosyncrasies of MATLAB make it less automated than would be desirable, however, and considerable human intervention is needed for complex solutions.

Together with the simulation program, high precision probes and data acquisition systems coupled with fitting and profile extraction software have allowed an excellent degree of confidence in identifying equilibrium states. The time resolved fit code permitted accurate identification of equilibrium states as well as time resolved examination of the turbulent formation phase and evolution. The profile extraction program, which is to our knowledge unique, has allowed very quick and accurate identification of the current and pressure profiles. The extraction program was able to detect plasma pressure and the precise form of λ profiles, revealing that even states which the fit code identified as constant λ in fact had small deviations on the order of 10% from constant λ and from zero pressure. Though this indicates that the spheromak is not quite

precisely in the predicted [Taylor, 1986] minimum energy state, it also indicates that small perturbations from this state are not important. This is an advantage both to fusion and reconnection applications, since in each case stability of the field is an asset.

This project concludes the equilibrium experiments on SSX. The lab will now move on to study the reconnection between two spheromaks like those described here. Two such spheromaks will be generated simultaneously and allowed to touch through small gaps cut in their flux conservers to study in detail the reconnection region (figure 12). The equilibrium measurement and fit system will remain in place during some reconnection experiments in order to monitor spheromak during reconnection in real time.

A Grad Shafranov Derivation

In order to simplify the plasma equilibrium equations, we consider the case in which the equilibrium has azimuthal symmetry about the z axis in a cylindrical coordinate system r, z, ϕ . In such a system, any physical quantity f has the characteristic $\frac{df}{d\phi} = 0$. This symmetry applies to most spheromaks as well as to many other magnetic confinement devices. Beginning with the full equilibrium equation:

$$\nabla P = \vec{J} \times \vec{B} \quad (9)$$

we look for the form that results when we substitute in axisymmetric forms of the B and J fields [after Bellan, unpublished course notes].

We begin with a statement of some useful vector identities, which are true for any quantity. Consider the scalars ϕ, Ψ , and the vector quantity \vec{F} . The curl of a gradient is always zero:

$$\nabla \times \nabla \phi = 0$$

Likewise, the divergence of a curl is zero:

$$\nabla \cdot \nabla \times \vec{F} = 0$$

Lastly, the divergence of the cross product of two gradients is also zero:

$$\nabla \cdot (\nabla \Psi \times \nabla \phi) = 0$$

Thus, we can always write:

$$\nabla \times \vec{F} = \nabla \Psi \times \nabla \phi$$

so that any quantity which can be written as the curl of a vector quantity can also be written as the cross product of the gradient of two scalars.

The magnetic field can be expressed as the curl of the vector potential, so we can take advantage of the formalism outlined above. In the axisymmetric case, is convenient to split the field into toroidal and poloidal components. We can then write:

$$\nabla \times \vec{A} = \vec{B} = B_{poloidal} + B_{toroidal} = B_p + B_t = \frac{1}{2\pi} [\nabla \Psi \times \nabla \phi + \mu_0 I_z \frac{\hat{\phi}}{r}]$$

where I_z, Ψ are functions only of r and z , not of toroidal angle. Here we have taken advantage of the vector identity to write B_p as the cross product of two gradients. Taking ϕ to be the toroidal angle, so that $\nabla \phi = \frac{\hat{\phi}}{r}$ guarantees that B_p is purely poloidal and is axisymmetric. Integration of the poloidal field yields:

$$\int B_p \cdot dA = \int_0^r \frac{1}{2\pi} [\nabla \Psi \times \nabla \phi] \cdot \hat{z} 2\pi r' dr' = \int_0^r \frac{d\Psi}{dr'} dr' = \Psi$$

so that Ψ is the poloidal flux. The toroidal field is simply given by Ampere's law, and is also axisymmetric. Writing the toroidal field in terms of $\nabla \phi$, we get:

$$B_p + B_t = \frac{1}{2\pi} [\nabla \Psi \times \nabla \phi + \mu_0 I_z \nabla \phi]$$

This is the most general form of the axisymmetric magnetic field. It is expressed in terms of the poloidal flux and I_z , which will be of use later on.

Having an expression for the field, we next look for the current, which we can find via:

$$\nabla \times \vec{B} = \mu_0 \vec{J}$$

So we calculate:

$$\frac{1}{\mu_0} \nabla \times B_t = \nabla \times \frac{1}{2\pi} I_z \nabla \phi = \frac{1}{2\pi} \nabla I_z \times \nabla \phi$$

which is purely poloidal. Now for the poloidal field, we have:

$$\frac{1}{\mu_0} \nabla \times B_p = \frac{1}{\mu_0} \nabla \times (B_r \hat{r} + B_z \hat{z}) = \frac{\hat{\phi}}{\mu_0} \left(\frac{dB_r}{dz} - \frac{dB_z}{dr} \right)$$

which is purely toroidal. Since it is purely toroidal, we can apply a vector triple product rule to obtain:

$$|\nabla \times B_p| = r \nabla \phi \cdot \nabla \times B_p = r \nabla \cdot (B_p \times \nabla \phi) = r \nabla \cdot \left(\frac{1}{2\pi} [\nabla \Psi \times \nabla \phi] \times \nabla \phi \right) = -\frac{r}{2\pi} \nabla \cdot \left(\frac{1}{r^2} \nabla \Psi \right)$$

so that:

$$\frac{1}{\mu_0} \nabla \times B_p = -\frac{r^2}{2\pi\mu_0} \nabla \cdot \left(\frac{1}{r^2} \nabla \Psi \right) \nabla \phi$$

which is again toroidal. Hence we have obtained the toroidal and poloidal components of \vec{J} :

$$J_p + J_t = \frac{1}{2\pi} \nabla I_z \times \nabla \phi - \frac{r^2}{2\pi\mu_0} \nabla \cdot \left(\frac{1}{r^2} \nabla \Psi \right) \nabla \phi$$

We can now evaluate the equilibrium equation using these fields and currents.

$$\nabla P = (J_p \times B_t) + (J_t \times B_p) + (J_p \times B_p)$$

Since J_t and B_t are parallel there is no $(J_t \times B_t)$ component. The last term of the above is zero since it is in the toroidal direction, so that:

$$J_p \times B_p = (\nabla I_z \times \nabla \phi) \times (\nabla \Psi \times \nabla \phi) = 0$$

This implies that ∇I_z is parallel to $\nabla \Psi$ and therefore that I_z is a function of Ψ :

$$\nabla I_z(\Psi) = I'_z(\Psi) \nabla \Psi$$

where ' indicates a derivative with respect to Ψ . Using this, we can re-write the poloidal current density, obtaining a current which is a function of Ψ :

$$J_p + J_t = \frac{I'_z}{2\pi} \nabla \Psi \times \nabla \phi - \frac{r^2}{2\pi\mu_0} \nabla \cdot \left(\frac{1}{r^2} \nabla \Psi \right) \nabla \phi$$

Now we can substitute our expressions for current and field in to the equilibrium equation, obtaining:

$$\begin{aligned} \nabla P &= (J_p \times B_t) + (J_t \times B_p) \\ \nabla P &= \left[\frac{I'_z}{2\pi} (\nabla \Psi \times \nabla \phi) \times \frac{\mu_0 I_z}{2\pi} \nabla \phi \right] - \left[\nabla \phi \frac{r^2}{2\pi\mu_0} \nabla \cdot \left(\frac{1}{r^2} \nabla \Psi \right) \times \frac{1}{2\pi} (\nabla \Psi \times \nabla \phi) \right] \end{aligned}$$

Again making use of vector triple product rules, we can reduce this to:

$$\nabla P = - \left[\frac{\mu_0 I_z I'_z}{(2\pi r)^2} + \frac{1}{(2\pi)^2 \mu_0} \nabla \cdot \left(\frac{1}{r^2} \nabla \Psi \right) \right] \nabla \Psi \quad (10)$$

indicating that P is also a function of Ψ . This allows us to write $\nabla P = P'(\Psi) \nabla \Psi$. Writing P in this form, equation 10 has a factor of $\nabla \Psi$ which can be divided out, leaving:

$$\nabla \cdot \left(\frac{1}{r^2} \nabla \Psi \right) + 4\pi^2 \mu_0 P' + \frac{\mu_0^2}{r^2} I_z I'_z = 0$$

which is the Grad Shafranov equilibrium equation.

B References

- C.W. Barnes, et al, "Experimental Determination of the Conservation of Magnetic Helicity from the Balance Between Source and Spheromak," *Phys Fluids* 29 (1986), p3415.
- P. Bellan, unpublished course notes.
- P.K. Browning, et al, "Relaxed and Partially Relaxed Magnetic Equilibria in Tight Aspect Ratio Tori," *Plasma Phys Control Fusion* 35 (1993), p1563.
- G.W. Hart, et al, "Finite Pressure Gradient Influences on Ideal Spheromak Equilibrium," *Phys Rev Lett* 51n7 (1983), p1558.
- T.R. Jarboe, "Review of Spheromak Research," *Plasma Phys Control Fusion* 36 (1994), p945.
- T.R. Jarboe, et al, "Motion of a Compact Toroid inside a Cylindrical Flux Conserver," *Phys Rev Lett* 45n15 (1980), p1264.
- D.A. Kitson and P.K. Browning, "Partially Relaxed Magnetic Field Equilibria in a Gun Injected Spheromak," *Plasma Phys Control Fusion* 32 (1990), p1265.
- S.O. Knox, et al, "Observations of Spheromak Equilibria Which Differ from the Minimum Energy State and Have Internal Kink Distortions," *Phys Rev Lett* 56n8 (1986), p842.
- Y. Ono, et al, "Experimental Investigation of Three Dimensional Magnetic Reconnection by use of Two Colliding Spheromaks," *Phys Fluids B* 5 (1993), p3691.
- M.J. Schaffer, "Exponential Taylor States in Circular Cylinders," *Phys Fluids* 30 (1987), p160.
- J.B. Taylor, "Relaxation of Toroidal Plasma and Generation of Reverse Magnetic Fields," *Phys Rev Lett* 33 (1974), p1139.
- J.B. Taylor, "Relaxation and Magnetic Reconnection in Plasmas," *Rev Mod Phys* 58 (1986), p741.
- F.J. Wysocki, et al, "Evidence for Pressure Driven Instability in the CTX Spheromak," *Phys Rev Lett* 65 (1988), p2457.
- M. Yamada, et al, "Magnetic Reconnection of Plasma Toroids with Cohelicity and Counterhelicity," *Phys Rev Lett* 65 (1990), p721.

C Acknowledgements

The author wishes to thank his advisor, Michael Brown, and fellow researcher Thomas Kornack for their help, ideas, and cooperation in this project. Their contributions have been invaluable. Financial support has been provided by the Department of Energy, Research Corporation, and the Petroleum Research Fund.